THE ASTROPHYSICAL JOURNAL, 316:546–572, 1987 May 15

THE RADIO MORPHOLOGY OF 3C 120 ON SCALES FROM 0.5 PARSECS TO 400 KILOPARSECS

R. C. WALKER
National Radio Astronomy Observatory[1] Socorro, New Mexico
J. M. BENSON
National Radio Astronomy Observatory[1] Charlottesville, Virginia
AND
S. C. UNWIN
Owens Valley Radio Observatory, California Institute of Technology
Received 1986 September 22; accepted 1986 October 28

ABSTRACT

The radio morphology of the Seyfert galaxy 3C 120 is shown on scales ranging from 0.5 pc to over 400 kpc. A jet is seen on all scales up to at least 100 kpc. On the larger scales an edge-brightened lobe is seen on the side opposite the jet, and diffuse structures are seen in several directions. The jet is one-sided and displays polarization characteristics indicative of a longitudinal magnetic field. The decrease in flux density per unit length of jet with distance from the core can be described by a power law for over five orders of magnitude in core distance. A power law is an even better approximation to the decrease in the central brightness of the jet with jet width, although good measurements of the jet width are available only over about three and one-half orders of magnitude. Fluctuations of over an order of magnitude are superposed on the overall decrease of either parameter so, without the uniquely wide range of scales available in these observations, the simple power-law dependence probably would have been missed. The simple dependence of brightness on distance implies that the physical parameters of the jet evolve in a simple manner. The power law of central brightness with jet width is such that, under the usual minimum-energy assumptions, the energy density times the cross-sectional area of the jet is about constant, and the magnetic field decreases inversely with the jet width. The superluminal motions seen in the inner few parsecs imply, by the standard model, that the velocity of the jet is relativistic on small scales. The lack of Faraday rotation, along with other arguments, suggests that thermal material is a relatively minor component of the jet, at least on parsec scales. There is still no clear evidence that gives interesting constraints on the velocity or density of the jet on large scales, although the data overall seem most consistent with a light, fast jet.

The continuous connection seen in 3C 120 between large-scale, linear structures and parsec scale regions with observed superluminal motions provides some of the best available evidence, although still circumstantial, that the structures generally referred to as jets in extragalactic radio sources actually contain moving material. The simple evolution of brightness along the jet suggests that the basic parameters of the jet are established on subparsec scales and are maintained to distances well outside the galaxy.

Subject headings: galaxies: individual (3C 120) — galaxies: jets — galaxies: Seyfert — interferometry — polarization — radio sources: galaxies

I. INTRODUCTION

The radio source 3C 120 is dominated by a highly variable, compact core that has been an object of intense study with VLBI for over a decade (Seielstad *et al.* 1979 and references therein; Walker *et al.* 1982). It is one of the few sources for which extensive observations of superluminal motions are available (above references; Walker 1984*a*; Walker *et al.* 1984; Walker *et al.* 1986, hereafter Paper I) and, being associated with a galaxy at $z = 0.033$, is the closest of the known superluminals. For $H_0 = 100$ km s^{-1} Mpc^{-1} and $q_0 = 0$, one mas (milliarcsecond) corresponds to 0.46 pc at the source. The source has long been known to have large-scale structure because it has high flux densities at low frequencies. However, the large-scale structure has been difficult to study at centimeter wavelengths because it is far weaker than the core. Soboleva *et al.* (1982) report the existence of extended emission up to about 1′ to either side of the core. Balick, Heckman, and Crane (1982) have reported observations of a jet structure on 1″–30″ scales. Schilizzi and de Bruyn (1983) and de Bruyn and Schilizzi (1984) have made high dynamic range observations with the Westerbork Synthesis Radio Telescope that show the presence of most of the large-scale features reported here, but, because of the low declination of 3C 120, they have such poor north-south resolution that much of the interesting structure is not apparent.

The galaxy associated with 3C 120 is generally classified as a Seyfert although it spiral nature is not certain (see discussion and references in Baldwin *et al.* 1980). The optical emission from the off-nuclear regions has been studied by Baldwin *et al.* They confirm the presence of stars at the same redshift as the nuclear emission lines, making any argument that "superluminal" motions are actually slower motions seen in objects with discrepant redshifts very difficult. They show that the velocity field of the galaxy, as seen in the forbidden lines, has a rotational component but is highly disturbed. There appears to be gas throughout the extent of the visible galaxy that is ionized by radiation from the nucleus. Wlerick *et al.*

[1] The National Radio Astronomy Observatory is operated by Associated Universities, Inc. under contract to the National Science Foundation.

(1981) and Arp (1981) have reported the presence of an optical jet in 3C 120. For at least the first few arcseconds this jet coincides approximately with the radio jet. In this region, the spectra shown by Baldwin *et al.* appear to be double-peaked. However, the linear structure roughly 10″ northwest of the core, that has been associated with the jet by Wlerick *et al.* and Arp (1986), is clearly separated from the radio jet.

The nuclear region of 3C 120 is a powerful and variable emitter of radiation at all observed frequencies. At X-ray frequencies, it has the unique property, relative to other Seyfert galaxies, that the spectral index varies with the intensity (Halpern 1984). At optical frequencies, variability is seen in both the continuum (see, e.g., Lyutyi 1979; Wlerick, Westerlund, and Garner 1979; Pollock *et al.* 1979) and the spectral lines (e.g., Oke, Readhead, and Sargent 1980). Variations are seen in the infrared but appear to be on longer time scales than at the radio, optical, and X-ray frequencies (Rieke and Lebofsky 1979). The radio source is highly variable (see, e.g., Epstein *et al.* 1982; Aller, Olsen, and Aller 1976 and references in both) and shows superluminal motions as discussed above. In most respects, 3C 120 resembles objects classified as QSOs. Because it is relatively nearby and because the nuclear region is not so bright that detailed studies of the underlying galaxy are precluded, it is potentially a very important source of information on the QSO phenomenon.

The observations presented in this paper show the radio morphology of 3C 120 on scales from 0.″1 to over 14′. They were made with the Very Large Array (VLA) of the National Radio Astronomy Observatory. Data were obtained using two configurations at 15 GHz and all four configurations at 1.4 and 5 GHz. The extended structures in 3C 120 are very weak relative to the central component, so very high dynamic range maps are required to show their morphology. To obtain the required dynamic range, closure offsets had to be calibrated. These are the first observations for which this calibration was successfully performed on VLA data. The maps of the extended features also benefited from the fortuitous circumstances that the highly variable central component was relatively weak during the observations. The VLA data are combined with VLBI results, the details of which will be presented in other papers under preparation (Paper I; Benson *et al.* 1986, hereafter Paper II) to show the evolution of the radio jet over five orders of magnitude in distance from the core.

In order to facilitate discussion of the full range of scale sizes in 3C 120, one of the best maps from the 5 GHz, VLBI monitoring program (Paper I) and two maps from the first large (14 stations) 1.6 GHz VBLI observations (Paper II), made with different tapers, are shown in Figure 1. The 5 GHz map shows several bright components near the eastern end of the source. These are the superluminal components discussed in Paper I. The easternmost feature is the one relative to which the others are moving and is assumed to be the stationary core. To the west of the brighter features is low-level emission with components up to 50 mas from the core. The coverage of short spacings in the 5 GHz experiments was sufficiently poor that little confidence can be placed in the exact details of the extended emission. However, comparison with the 1.6 GHz maps shows a good correspondence between features in the maps and lends credibility to them. The 1.6 GHz map does not resolve well the superluminal components but shows a jetlike structure extending up to 250 mas from the core. The jet broadens and weakens with distance and shows a number of bends and knots. The details, along with comparison with a somewhat better, second epoch map will be discussed in Paper II. The 1.6 GHz maps have higher dynamic range and show more complex structure than most other VLBI maps made to date.

II. THE OBSERVATIONS

Some of the 5 GHz monitoring VLBI experiments to be reported in Paper I (Fig. 1 is an example) showed the presence of emission on scales of tens of mas in the direction toward which the superluminal components are moving. These features induced us to propose large, 1.6 GHz VLBI observations (Paper II; preliminary results are presented in Benson *et al.* 1984) and to analyze the VLA data that were obtained as an incidental byproduct of the use of the phased array as one element of the VLBI interferometer. Approximately half of the VLA observations reported here were made during such VLBI observations. The results of these lower resolution observations were so interesting that further VLA observations were proposed in the conventional manner to cover resolutions and frequencies that were missed during the VLBI sessions and to obtain polarization data that could not be calibrated for phased array data during the earlier observations (polarization data can be calibrated for phased array data taken since 1983).

The observations are summarized in Table 1. The columns of the table give (1) the date of the observations, (2) the frequency, (3) the VLA configuration, and (4) the resolution. Other than the phasing that was occurring for the VLBI runs, the observations were made in the normal continuum mode for the VLA. Details of the performance and operation of the VLA can be found in Thompson *et al.* (1980).

The calibration procedure used for the observations differed in several respects from the usual procedure. The traditional calibration, involving frequent observations of a nearby point source, was not done. Often 3C 120 was observed for hours at a time without interruption, especially during the VLBI experiments. The first cut at phase calibration was accomplished in one of two ways. For the VLBI runs, the online computers were adjusting the antenna phases in real time to give approximately zero phase on all VLA baselines. This was required to form the analog sum used as the signal to be recorded on the VLBI tapes. For the conventional VLA runs, observations of a strong source such as 3C 84 were made every hour or two in order to obtain paralactic angle calibration for polarization and in order to obtain closure calibration as will be discussed below. These scans were used for a first-cut phase calibration in the conventional manner, although the quality of that cali-

TABLE 1

SUMMARY OF VLA OBSERVATIONS

Date (1)	Frequency (MHz) (2)	VLA Conf. (3)	Resolution (4)
1983.75.....	1452.4	A	1.″26
1982.78.....	1664.3	B	3.84
1984.27.....	1665.0	C	11.8
1984.76.....	1464.9	D	37.5
1983.75.....	4885.1	A	0.37
1982.57.....	4985.0	B	1.26
1981.92.....	4985.0	C	3.84
1984.30.....	4885.1	C	3.85
1982.92.....	4985.0	D	11.8
1983.75.....	14964.9	A	0.11
1984.30.....	14914.9	C	1.26

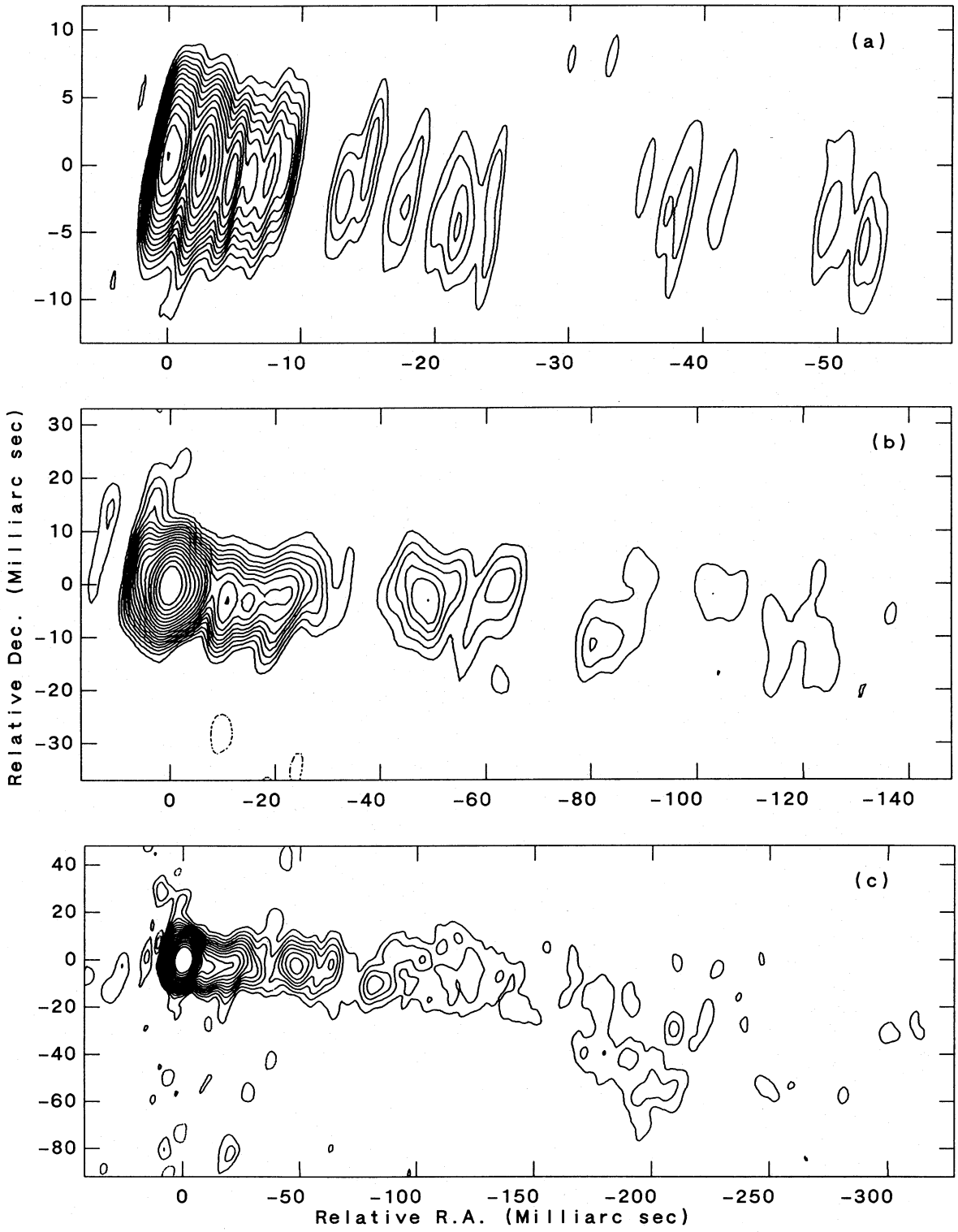

FIG. 1.—VLBI maps of 3C 120 taken from Papers I and II. (*a*) Map based on 11 station, 5 GHz VLBI data taken in 1982 December (Paper I). The bright components at the eastern end of the source are the superluminal components discussed in Paper I. The easternmost component is assumed to be the core. The restoring beam is 0.84 by 6.1 mas, elongated in position angle (P.A.) −10°. The contour levels are −13, −8, −4, 4, 8, 13, 19.3, 26.8, 37.3, 51.8, 72, 100, 139, 193, 268, 373, 518, and 720 mJy per beam. As with all contour plots in this paper other than the polarization plots, most of the contour levels are logarithmic with seven levels per decade. Also, all maps in this paper have the residual map added to the convolved CLEAN components—the usual practice for linked interferometers but not necessarily for VLBI. (*b*) Map based on 14 station, 1.6 GHz VLBI data taken in 1982 October (Paper II). The restoring beam is 3.0 by 8.0 mas, elongated in P.A. −11°. The contour levels are the same as in Fig. 1*a* with a level at 1000 mJy per beam added. The scale is also the same as Fig. 1*a* to aid comparison. Note that absolute position information is lost in VLBI maps so the true registration of the maps is not precisely determined. (*c*) Map based on the same data as Fig. 1*b* but with a taper applied. The convolving beam is 5.1 by 9.8 mas, P.A. −11°. The contour levels are −6.6, −4.0, −2.0, 2.0, 4.0, 6.6, 10.0, 13.9, 19.3, 26.8, 37.3, 51.8, 72, 100, 139, 193, 268, 373, 518, and 720 mJy per beam.

bration was limited by the infrequency of the scans and the large separation between the calibrator and 3C 120.

The amplitudes for most of the observations at 1.4, 1.6, and 5 GHz were calibrated in the normal manner for the VLA by using 3C 286 or 3C 48 and the flux density scale of Baars *et al.* (1977). For observations calibrated in this manner, the errors in the amplitudes of individual, off-core features, which are all very weak relative to the core, are probably dominated by effects introduced by the map-making process. Comparison of two 5 GHz maps based on data from different epochs with very different core flux densities suggests that such errors are about 5% on the extended features. The amplitudes for three of the observations, 1.6 GHz in 1982.78 and 5 GHz in 1981.92 and 1982.92, were calibrated based on the 3C 120 total flux density measurements made at Bonn as part of the calibration of the VLBI observations being made at the same time. These measurements are also based on the Baars flux density scale, but the indirect calibration of the VLA data is less reliable than when proper VLA calibration scans were made. (During these early VLBI observations, the usefulness of the VLA phased array data was not fully appreciated so no special efforts were made to calibrate it.) The amplitudes from these epochs probably should not be trusted to better than 10%. The 15 GHz data were calibrated based on 3C 286 and the Baars scale. However, bad weather and other problems that are not fully understood produced a measured 3C 120 flux density in 1983.75 that was not consistent (too low) with other measurements at similar epochs. Since the VLA calibration was not trusted at 15 GHz for that epoch, the data were scaled to give a total flux density that matched that measured at the University of Michigan at about the same time (H. D. and M. F. Aller, private communication). The absolute flux densities of components in that observation probably should not be trusted to better than about 15%. The polarization data were calibrated in the usual manner assuming position angles of 33° at all frequencies for 3C 286 and $-12°$ at 1.4 and 5 GHz and $-18°$ at 15 GHz for 3C 138.

The final calibration of the data relied heavily on the self-calibration algorithm of Schwab (1980) and was done within the Astronomical Image Processing System (AIPS) at NRAO. The technique is very similar to that used in mapping of VLBI data (cf. Readhead and Wilkinson 1978). After initial calibration as described above, a map was made and CLEANed (Hogbom 1974). The CLEAN components were examined, and the level at which spurious components first appeared was determined. Here spurious components are ones that are well outside the regions in which emission was expected based either on the CLEAN map or on previous maps. The components above this level were then used as the input model for the next iteration of self-calibration. For the first few iterations, only phase adjustments were made. After that, both the amplitudes and phases were corrected. At some point early in this process, corrections were made for nonclosing errors as described in the Appendix. Such errors limit the dynamic range and, for low declination sources such as 3C 120, cause serious degradations to the north and south of bright features such as the core.

The maps shown in this paper required between seven and 19 iterations of self-calibration before the improvements in the noise level in the map from one iteration to the next were so small that further iterations were deemed not worthwhile. For most of the maps, the input data set at each iteration was either one that had not been self-calibrated or one that had been self-calibrated once. It is not clear that this is important, but it does minimize any tendency for the position or flux density to drift with successive iterations. It should be noted that the above procedure will result in a position for the source that matches the coordinates assumed for the observing. For a source such as 3C 120, which is a VLA calibrator (!) with a very well known position, this is not important. Dynamic ranges, measured as the ratio of peak to off-source rms, in excess of 30,000 were reached in some maps, compared to a maximum of about 10,000 that is possible without the closure corrections. These were the highest dynamic ranges achieved with the VLA at the time the maps were made, although they have been surpassed since by experiments in which careful attention was paid to minimizing the closure errors during the observations. The above numbers are based on off-source rms values measured over regions constituting between one-tenth and one-third of the total map area and located outside any tight CLEAN windows that might have been used. If the full inner quarter of the map was CLEANed, the rms measurement region was partially within the clean window.

III. THE RESULTS

The maps will be described in order of decreasing resolution. The maps are all displayed with logarithmic contours above the second or third level. There are seven contours per order of magnitude so the contours are spaced by a factor of 1.39. The lowest level was chosen to show just enough of the noise to give a feeling for the quality of the map but not so much that the source structure is camouflaged. In most maps, the second contour is twice the first and the third is at a level somewhat more than 3 times the first and chosen to give a smooth transition to the logarithmic levels to follow. The highest contour in the VLA maps is not in the logarithmic sequence. It is set at half the peak brightness in the map. In the VLA maps, as opposed to the VLBI maps where the core is resolved, the core is not resolved at greater than about 5% of the peak. Therefore the highest contour is an accurate representation of the half-power level of the convolving beam.

In cases where there are maps at more than one frequency at a given resolution, the contours for one map have been set as described above. At the other frequencies, the contour levels have been scaled by a spectral index of $\alpha = -0.65$ ($S \propto \nu^{\alpha}$). In cases where the lowest of the scaled levels is too deep in the noise, the corresponding contour has been omitted. These are the maps in which the logarithmic scheme begins above the second level. With this scheme, if the spectral index used for scaling is the same as that of the source, the maps at different frequencies should look the same, ignoring any unmatched lowest contour. The value used for scaling was chosen to be close to the average spectral index along the center of the jet between about 2".5 and 3' from the core. The average of 104 such points was found to be -0.64 with an rms scatter of 0.12, probably due mostly to noise.

The polarization maps display the electric field vectors. The vectors can be assumed to be approximately perpendicular to the magnetic field. The length of the polarization vectors is proportional to the percentage polarization. The percentage polarization is smaller on the core than along the jet or in the lobes, but the core is so bright that the polarized flux density is dominated by the core. The polarization vectors have not been corrected for Faraday rotation. However, as will be shown, any such rotation in 3C 120 is small and does not significantly affect the results.

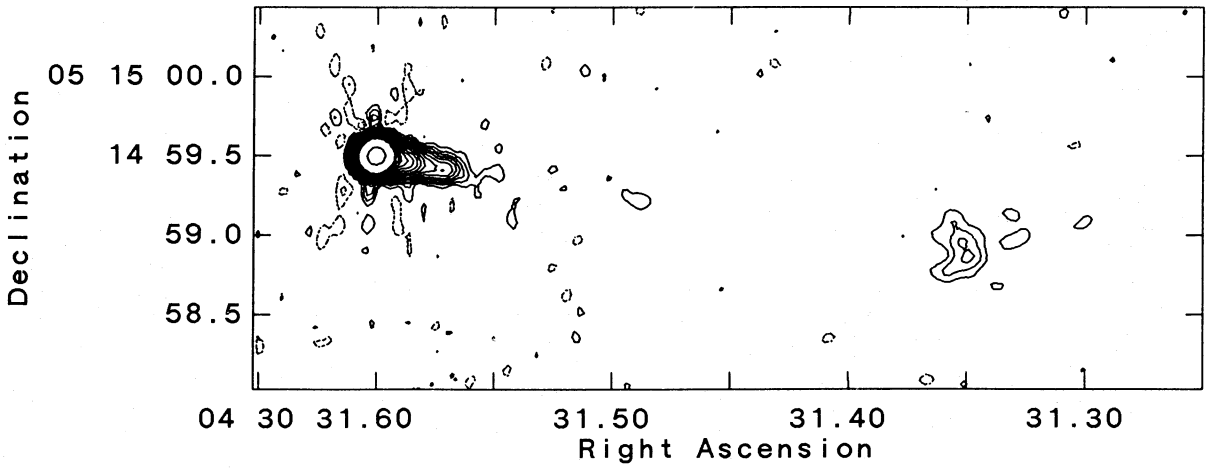

FIG. 2.—VLA map made at 15 GHz using the A-configuration. The convolving beam is nearly circular with a full width at half-maximum (FWHM) of 0.″11. Here, and in all following figures, "nearly circular" means that the axial ratio is within 1% of 1.0. The contour levels are −1.9, −1.2, −0.6, 0.6, 1.2, 1.9, 2.68, 3.73, 5.18, 7.20, 10.0, 13.9, 19.3, 26.8, 37.3, 51.8, 72.0, 100, 139, and 881 MJy per beam, and the peak flux density in the map is 1.76 Jy per beam. The highest contour is at the half-power point of the core and, as in all of the VLA maps, is a good representation of the beam.

Many of the maps show low-level "ears" and other structures near the core. These are spurious features and are evidence that the closure corrections are not perfect. Maps made without the closure corrections show similar features at much higher levels. Features at flux densities similar to that of these spurious features, but located far from the core, especially to the east and west, represent real emission and repeat in different observations and at different frequencies. An example is seen in Figure 2, the first map to be discussed below. Calibration artifacts are seen just north and south of the core at the same flux density level as the real knot at about 4″ to the west of the core.

a) The Highest Resolution VLA Maps

The highest resolution VLA map was made at 15 GHz using the A-configuration. An untapered version is shown in Figure 2. It shows an extension (it actually qualifies as a jet under the criteria of Bridle and Perley [1984]) in the same direction as the VLBI jet. In fact, the largest scale features in the low-resolution, 1.6 GHz VLBI map (Fig. 1*c*) would be resolved in the 15 GHz VLA map, but the difference in resolutions is sufficiently great that there is a regime at a few hundred mas where the structure of the source is not determined in detail. This is the largest gap in our coverage of the structure of 3C 120 from 1 mas to about 14′. The jet clearly decays rapidly with distance from the core until it cannot be seen above the noise at about 0.″6. A knot appears at about 4″ that is elongated perpendicular to the jet. The polarization is shown in Figure 3. Very little Faraday rotation is seen even at the low frequencies so the data show that the magnetic field is parallel to the jet. The dynamic range is not sufficient to measure the polarization on the 4″ knot. A tapered version of the 15 GHz map was made that shows the continuous connection between the core and the 4″ knot, but that map contains no information not in the 5 GHz, A-array map and so is not shown.

The next step in resolution is to the 5 GHz, A-array map shown in Figure 4. Both a full resolution version and a tapered version, that brings up some of the lower level emission, are shown. The polarization information is shown in Figure 5. The jet is now seen to be continuous from the core to well beyond

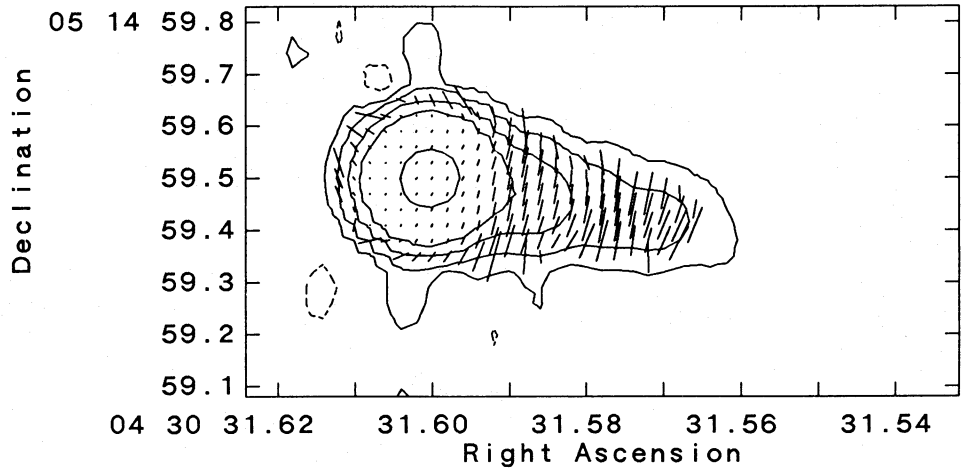

FIG. 3.—The polarization structure in the central region of the map of Fig. 2. The polarization vectors represent the direction of the electric field. The lengths of the vectors are proportional to the percentage polarization, with a length of 0.″1 corresponding to 48%. The percentage polarization is small on the core, but the core is so strong that the total polarized intensity is still dominated by the core. The contour levels are −1, 1, 4, 15, 50, and 881 mJy per beam.

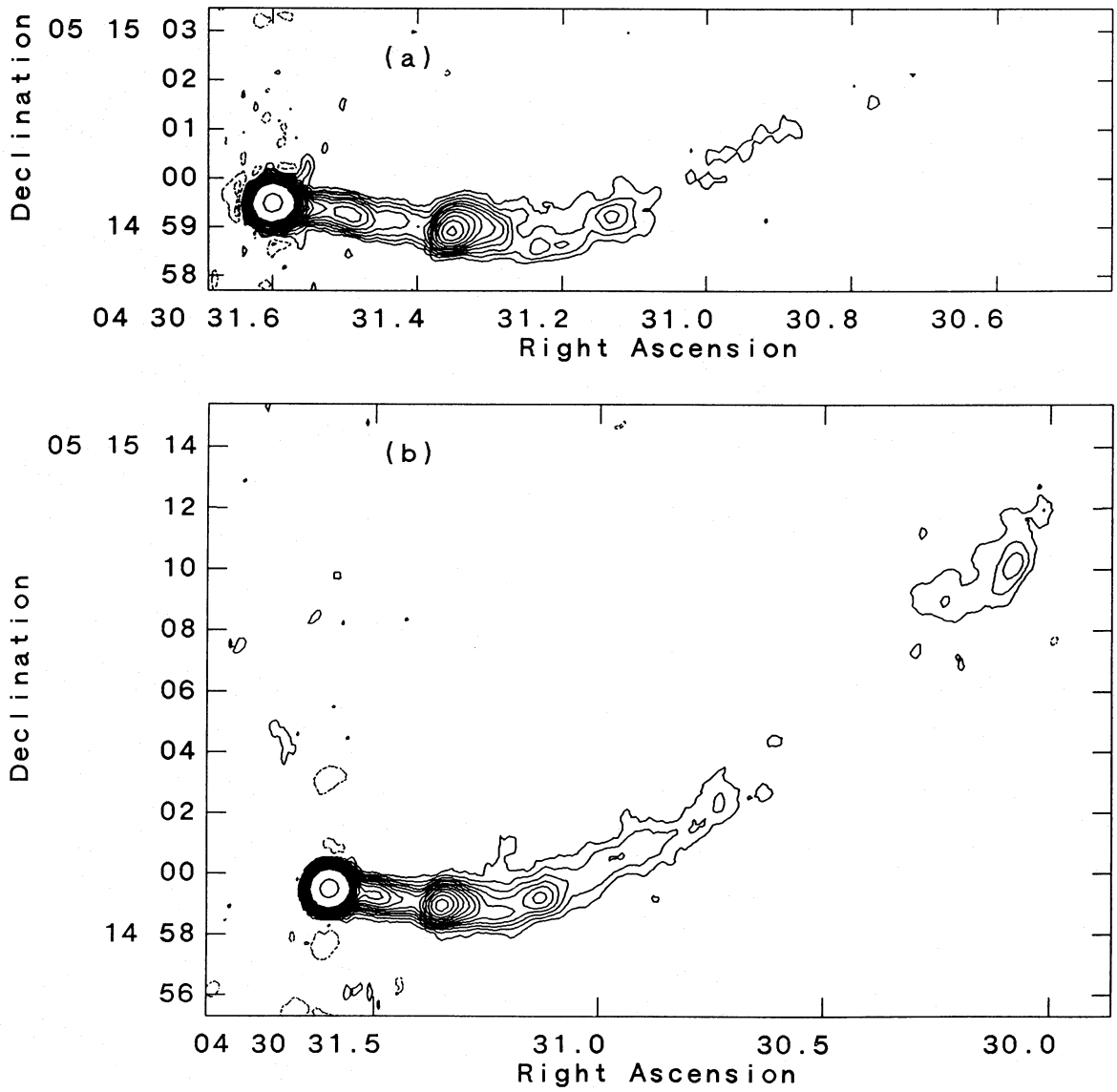

FIG. 4.—VLA maps made at 5 GHz using the A-configuration. (*a*) An untapered map for which the convolving beam is nearly circular with FWHM of 0".37. The contour levels are −1.3, −0.8, −0.4, 0.4, 0.8, 1.3, 1.93, 2.68, 3.73, 5.18, 7.20, 10.0, 13.9, 19.3, 26.8, 37.3, 51.8, 72.0, 100, and 964 MJy per beam, and the peak flux density in the map is 1.93 Jy per beam. (*b*) A tapered version of the map in (*a*). The convolving beam is nearly circular with a FWHM of 0".60. The contour levels are the same as in (*a*) except that the highest contour is 986 mJy and the peak in the map is 1.97 Jy per beam.

the 4" knot and a new knot is seen beyond the visible jet at about 20". The jet between the core and the 4" knot shows a slight double-bend structure that repeats on other maps including one made at 1.6 GHz with MERLIN at the time of the second epoch 1.6 GHz VLBI observations to be reported in Paper II.

The 4" knot shows a rather curious structure. It is brightest to the southeast with a more resolved structure curving away, first to the northwest and then bending back around to the southwest. The polarization is much stronger on the southern side of the knot than to the north—in fact the northeast corner is almost unpolarized. The polarization direction remains parallel to the overall jet structure through the knot, a situation that might not be expected for a shock and different from what is seen, for example, in the brightest knot of M87 (Owen, Hardee, and Bignell 1980). It is not clear what the 4" knot is. It could be the site of enhanced emission in the jet, or it could be just a location where a slightly curving jet that is nearly along the line of sight passes through the line of sight. The excess brightness in the latter case would be due to some combination of the extended line of sight through the jet and relativistic beaming. The 3C 120 jet is thought to be near the line of sight, at least near the core, because of the observed superluminal motions. However, such a geometry might not be expected to show the uniformly longitudinal magnetic field that is observed. Note that the half-width of the jet narrows at the knot (remember, the contours are logarithmic). It is possible that the enhanced brightness is just an effect of a decreased volume of the jet at that point if both the magnetic field is compressed and the particle density is increased. In fact, it will be shown later that the energy content per unit length of the jet remains roughly constant throughout. Any compression of a high Mach number jet should produce shocks so the actual situation is probably complicated.

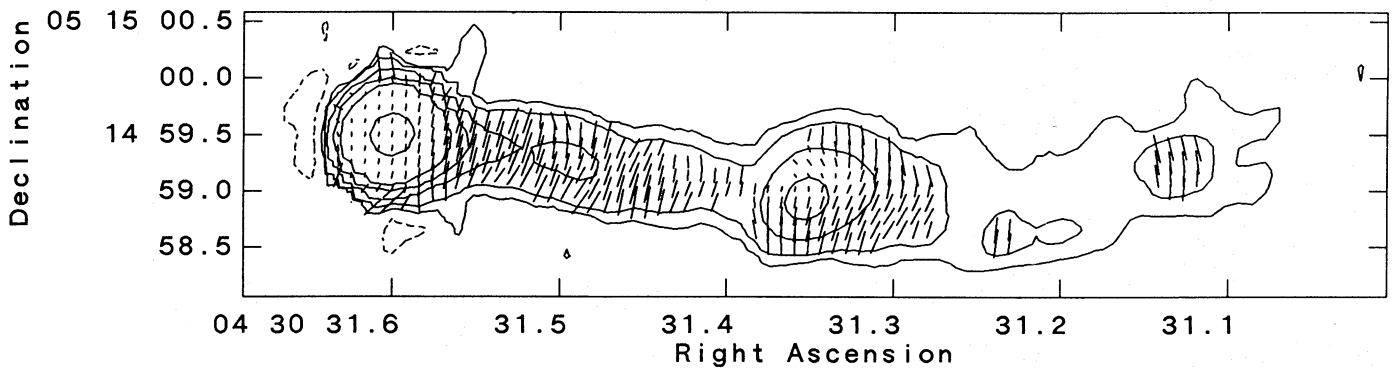

FIG. 5.—The inner region of the map of Fig. 4*a* but showing the polarization vectors. The polarization vectors are scaled so that a 0".5 vector corresponds to 60% polarization. The contour levels are −0.5, 0.5, 1.2, 5, 15, 50, and 964.5 mJy per beam. Note the strong gradient of percentage polarization across the knot 4" from the core. The dynamic range is not as high adjacent to the core as in other parts of the map so some of the polarization vectors near the core, especially those with discrepant directions, should be considered spurious.

The feature interpreted as a jet in the optical images of Wlerick *et al.* (1981) and Arp (1981) lies at about the location of the 4" knot, perhaps offset slightly to the north. If the optical emission is evidence of dense gas in or near the knot, perhaps it accounts for the low polarization seen in the northern part of the knot.

Beyond the 4" knot, the jet bends toward the northwest. At the bend, the emission is concentrated on the outside of the bend. This may be evidence for interaction between the jet material and the external medium. At about 20" there is a bright region that is extended along the extrapolation of the jet. The portion of this region closest to the core is extended to the east of the extrapolation of the jet. This is more apparent in lower resolution maps that follow. The jet is sufficiently weak just before the 20" region that no maps with sufficient resolution show whether it connects at the eastern or western end of the eastern extension. In fact, the 1.4 and 5 GHz maps shown below give conflicting indications, but the features involved are at such low levels that they are not reliable. It is possible that the jet is sufficiently broad to connect with the whole of the extension. Note that both the 4" knot and the 20" knot are seen in the maps of Schilizzi and de Bruyn (1983).

b) Maps with 1".26 Resolution

Figure 6 shows maps made at 1.4, 5, and 15 GHz, all with a resolution of 1".26. They were made with data from the A-, B-, and C-configurations, respectively. The contours have been scaled by the spectral index −0.65, and the lowest scaled contour in the 15 GHz map has been omitted. The differences between the maps, and hence any deviations from the mean spectral index, are not significantly above the level of fluctuations that could be caused by noise and calibration errors.

The polarization data at 1".26 resolution at 1.4 and 15 GHz are shown in Figure 7. As at smaller scales, the polarization shows that the magnetic field is parallel to the jet. As it happens, this is the only resolution at which polarization data are available at two frequencies. The Faraday rotation is small (0 to -10 rad m^{-2}) as is any depolarization. Since the rotation measure is small, the 15 GHz map shows the intrinsic polarization angles; the 1.4 GHz polarization vectors are rotated slightly but generally by less than 20°. The rotation between the 15 GHz and 1.4 GHz maps is less than 5° on the core and on the brightest portions of the 4" knot. In the brightest regions where the measurements are most reliable, the percentage polarization differs between maps by less than about 20% of the local value. The largest differences are about a factor of 2 where there is significant signal (note that on the north side of the 4" knot, the percentage polarization is higher at 1.4 GHz than at 15 GHz). Since the closure calibration could not be performed on the polarization data and the largest differences in polarization are in weak regions adjacent to the core, those differences could be the result of calibration problems.

c) Maps with 3".8 Resolution

Maps with 3".8 resolution are shown in Figures 8 through 10. Figures 8 and 9 show the total intensity at 5 GHz and 1.6 GHz, respectively. They show yet another knot about 1'.3 from the core along the generally curving line of the jet. They also show an edge-brightened lobe to the southeast of the core, in the opposite direction from the jet. Both of these features are apparent in the maps of Schilizzi and de Bruyn (1983), and the details agree as well as can be expected given the limited north-south resolution of the Westerbork observations. The 1.6 GHz map shows the first hints of more structure up to 3' to the north of the core. This structure is far more apparent in the lower resolution maps to follow.

The contour levels of Figures 8 and 9 are scaled by the spectral index except that the lowest contour has been left off Figure 8. Again, the similarity of the maps indicates that there is little significant deviation from the assumed spectral index over most of the source, including the southeast lobe (although the 5 GHz map appears noisier in that region). This is a rather flat spectral index for a classical lobe (cf. Miley 1980) but is characteristic of jets. The maps shown so far indicate that the spectral index is close to −0.65 (deviations are less than about 0.2) from about 3" to over an arcminute from the core. The lower resolution maps below will begin to show the steepening that might be expected from a decaying electron energy spectrum, but that steepening only happens very far from the core. Spectral index information is not available on the subarcsecond scales but analogy with the higher signal-to-noise ratio data on other superluminal sources (Unwin *et al.* 1983; Unwin *et al.* 1985) suggests that the spectral index is likely to be within ±0.3 of −0.65 a few mas of the core. If so and if that spectral index holds on scales between a few mas and a few arcseconds, the spectral index remains constant over a very wide range of size.

Thanks to the fact that the VLBI experiments are not timed to correspond to particular VLA configurations, there are two 5 GHz, C-configuration data sets. They were made at times

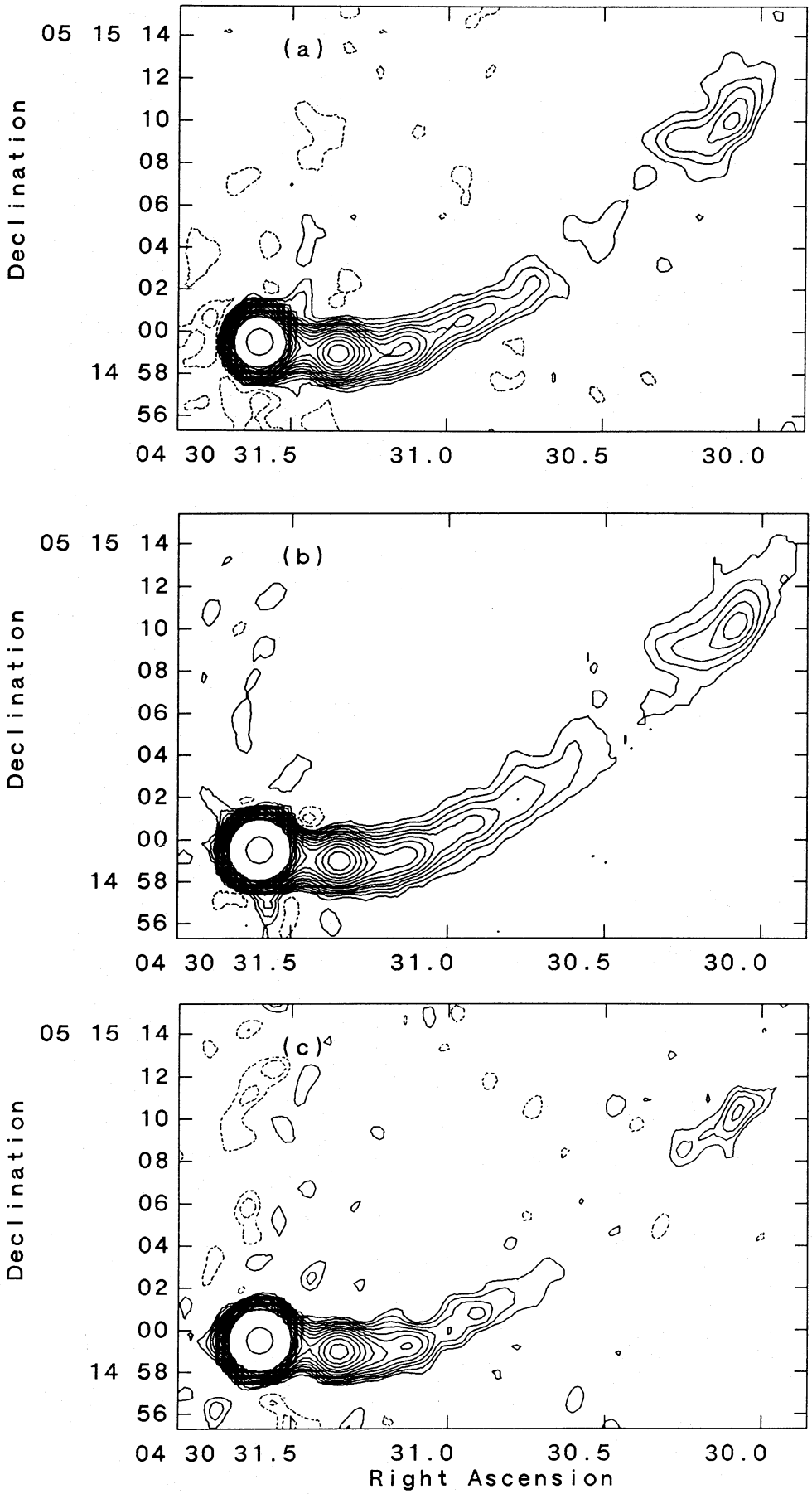

FIG. 6.—Three maps at different frequencies of the structure of 3C 120 with a resolution of just over 1″. The convolving beam in all three has a FWHM of 1″25. The contour levels have been scaled by a spectral index of $\alpha = -0.65$, except the contour corresponding to the lowest in the 1.4 and 5 GHz maps has been omitted from the 15 GHz map. With this contouring scheme, the maps would appear the same to within the noise if the spectral index is −0.65. Note that above the third contour (excluding the top contour, which is at the half-power point), a difference of one contour between maps spread by a factor of 3 in frequency corresponds to a spectral index difference of approximately 0.3. (*a*) Map made with 1.4 GHz, A-configuration data taken in 1983 October. The contour levels are −2.90, −1.78, −0.89, 0.89, 1.78, 2.90, 4.30, 5.98, 8.31, 11.6, 16.0, 22.3, 31.0, 43.0, 59.8, 83.1, 115, 160, 223, and 1385 mJy per beam, and the peak flux density in the map is 2.71 Jy per beam. (*b*) Map made with 5 GHz, B-configuration data taken in 1982 July. The contour levels are −1.3, −0.8, −0.4, 0.4, 0.8, 1.3, 1.93, 2.68, 3.73, 5.18, 7.20, 10.0, 13.9, 19.3, 26.8, 37.3, 51.8, 72.0, 100, and 1668 mJy per beam, and the peak flux density in the map is 3.28 Jy per beam. (*c*) Map made with 15 GHz, C-configuration data taken in 1984 April. The contour levels are −0.64, −0.39, 0.39, 0.64, 0.95, 1.32, 1.83, 2.54, 3.53, 4.90, 6.81, 9.47, 13.2, 18.3, 25.4, 35.3, 49.0, and 988 mJy per beam, and the peak on the map is 1.94 Jy per beam.

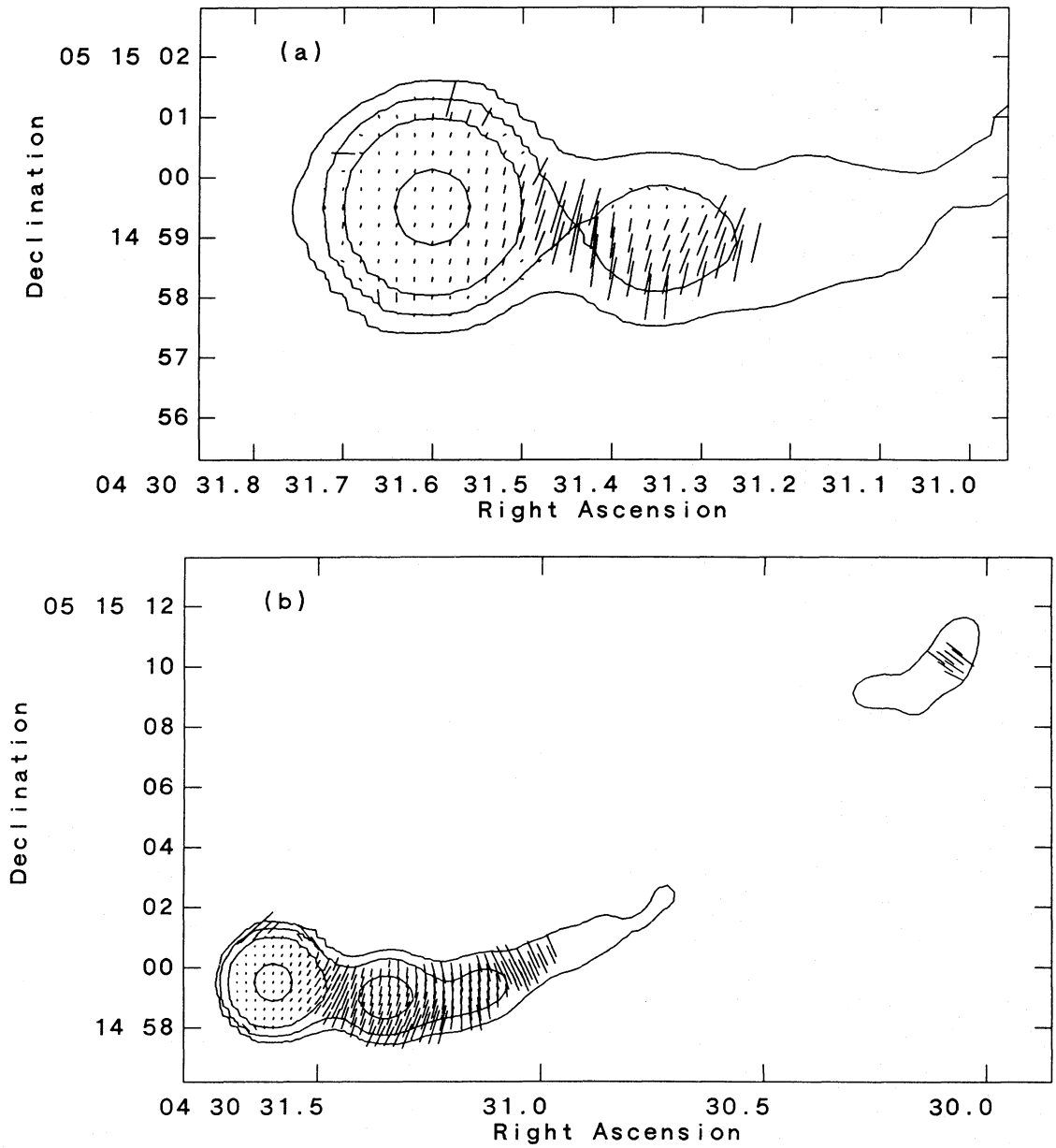

FIG. 7.—The polarization data at 1.4 and 15 GHz with a resolution of 1".25. The maps are the same as those in Fig. 6*a* and 6*c*. On both maps, a 1" polarization vector represents 42% polarization. No Faraday rotation has been removed, so the similarity of the polarization position angles on the two maps shows the lack of significant Faraday rotation. Only the regions in which polarized flux density was detected are displayed. Since the extended structure is much weaker at 15 GHz, the polarized flux density is also weaker at that wavelength, and the region over which it was detected is much smaller. As in all polarization maps in this paper, the vectors at low-flux density adjacent to the core are not reliable. The contour levels in the 15 GHz map are −1, 1, 7, 50, and 988 mJy per beam. In the 1.4 GHz map, they are −2.9, 2.9, 10, 50, and 1385 mJy per beam.

when the core flux density was rather different; 2.03 Jy in the map shown and 3.51 Jy in the other (1981 December). Comparison of the two maps shows very good agreement and lends confidence to even fairly minor details of the maps. Except for the spurious features in the immediate vicinity of the core and to the north and south of the core, the contours reproduce at a level much better than the interval between contours. The map shown has slightly lower noise and lower level spurious features, as expected because the core flux density is lower so the dynamic range required for a given noise level is not as high.

Figure 10 shows the polarization structure at 3".8 resolution at 5 GHz. No attempt has been made to remove Faraday rotation—given the results at 1".26 resolution it is likely that any such rotation is very small. The magnetic field in the jet is still parallel to the jet on these scales except that, in the knot at 1'.3, the field is rotated to an oblique angle relative to the jet direction. The magnetic field in the brighter part of the southeast lobe is parallel to the edge of the lobe. These characteristics will be discussed more fully after the 11".8 resolution maps are shown.

d) Maps with 11".8 Resolution

Maps with a resolution of 11".8 are shown in Figure 11. These maps were made at 5 and 1.6 GHz using the D- and

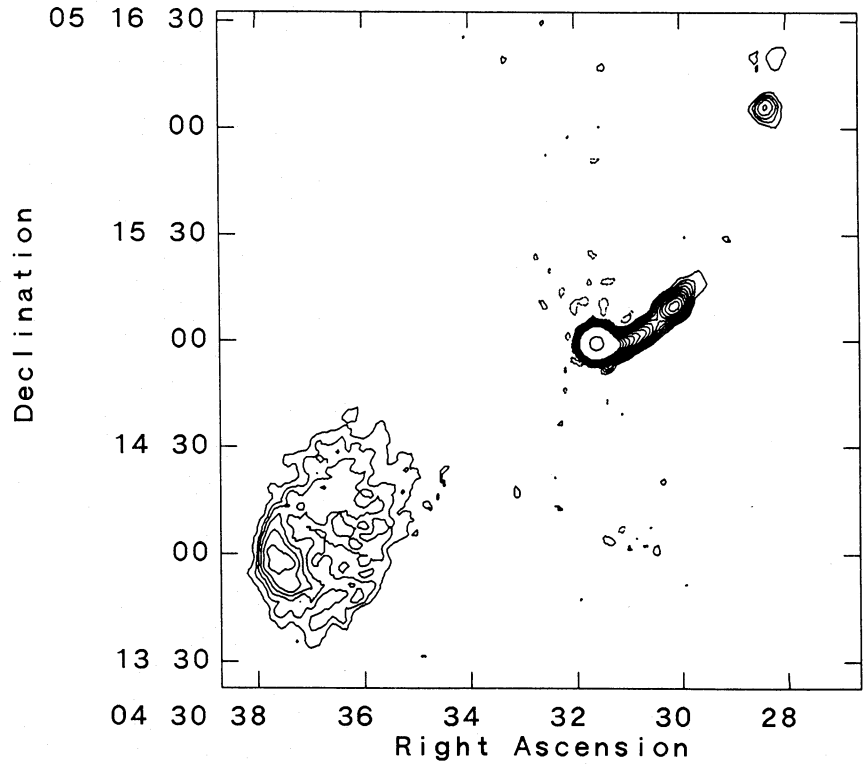

FIG. 8.—The VLA map of 3C 120 at 5 GHz based on data from the C-configuration taken in 1984 April. The convolving beam is nearly circular with a FWHM of 3.″84. The contour levels are −0.50, −0.30, 0.30, 0.50, 0.69, 1.33, 1.85, 2.57, 3.57, 4.97, 6.90, 9.59, 13.3, 18.5, 25.7, 35.7, and 1014 mJy per beam, and the peak flux density in the map is 2.03 Jy per beam.

C-configurations of the VLA, respectively. They show the jet continuously connected out to 3′ to the north of the core. At the greater distances from the core, the jet structure is becoming somewhat broken and diffuse. Also at 1.6 GHz, the first evidence of emission off to the sides of the jet and to the south of the core is seen. Here this emission is distinguished from noise and calibration problems only by the fact that it is uniformly positive over a large region. In a tapered version of the map (not shown), and in the lower resolution map to be discussed below, the emission is clearly real. The contours in the maps have been scaled by the spectral index, except that the lowest scaled contour has been left off the 5 GHz map. A steepening of the spectral index is seen in the region 3′ north of the core and in the more diffuse regions, although the noise makes detailed comparisons difficult. In these maps, the jet appears to end abruptly at about 3′ from the core. However, it will be shown below that the brightness just decreases at this point, but the structure does not end.

The polarization structure at 1.6 GHz at 11.″8 resolution is shown in Figure 12. In most areas, the field is still parallel to the jet. However, as at 5 GHz at higher resolution, the leading edge of the knot at 1.′3 shows a rotated field. The field angle is similar at 1.6 and 5 GHz so the rotation is intrinsic rather than due to Faraday rotation. Perhaps the knot is a shock, and the effects of compression of the fields along the direction of jet are being seen. However, high-resolution observations of M87 have shown that similar field configurations seen at low resolution are the result of more complex structures (F. N. Owen, private communication). In the lobe, the polarization intensity varies considerably, and the magnetic field direction shows a generally circumferential character. In the region where the polarization was measured at 5 GHz at higher resolution (Fig. 10), any Faraday rotation is less than about 20°, while the percent polarization at 1.6 GHz is at least $\frac{2}{3}$ of that at 5 GHz.

The nature of the southeast lobe is not clear. The circumferential magnetic field and edge-brightened lobe are similar to the structures seen in other extragalactic radio sources where a jet is thought to be impinging on the extragalactic medium (cf. Miley 1980; Begelman, Blandford, and Rees 1984; Linfield and Perley 1984). However, the brightest region is not as compact as the hot spots in many such sources, the spectral index is more characteristic of a jet than of a lobe, and the sharp outer boundary of the brightest region might not be expected if that region is the hot spot at the end of a line-of-sight jet. In that geometry, which is suggested by the superluminal motions, one might expect to see a hot spot projected more toward the middle of the associated diffuse lobe. An alternate possibility is that the southeast lobe is actually the counterjet. The bright region would be where it first becomes visible, perhaps because it has slowed enough that Doppler boosting is no longer important. At that point it is just bending through the line of sight. The more diffuse portions of the "lobe" could just be more distant portions of the jet where it has expanded. This would explain naturally the observed spectral index of the "lobe."

Comparison of Figure 11 with optical images reveals an intriguing superposition of an apparent nearby galaxy and the jet at about 2′ northwest of the core. The nearby galaxy is the largest other than 3C 120 in the vicinity and is clearly seen in the image published by Arp (1981). The center of the jet passes directly over the center of the galaxy within the measurement errors of a few arcseconds (the comparison was made with an optical CCD image kindly provided by Dr. F. Owen). It is

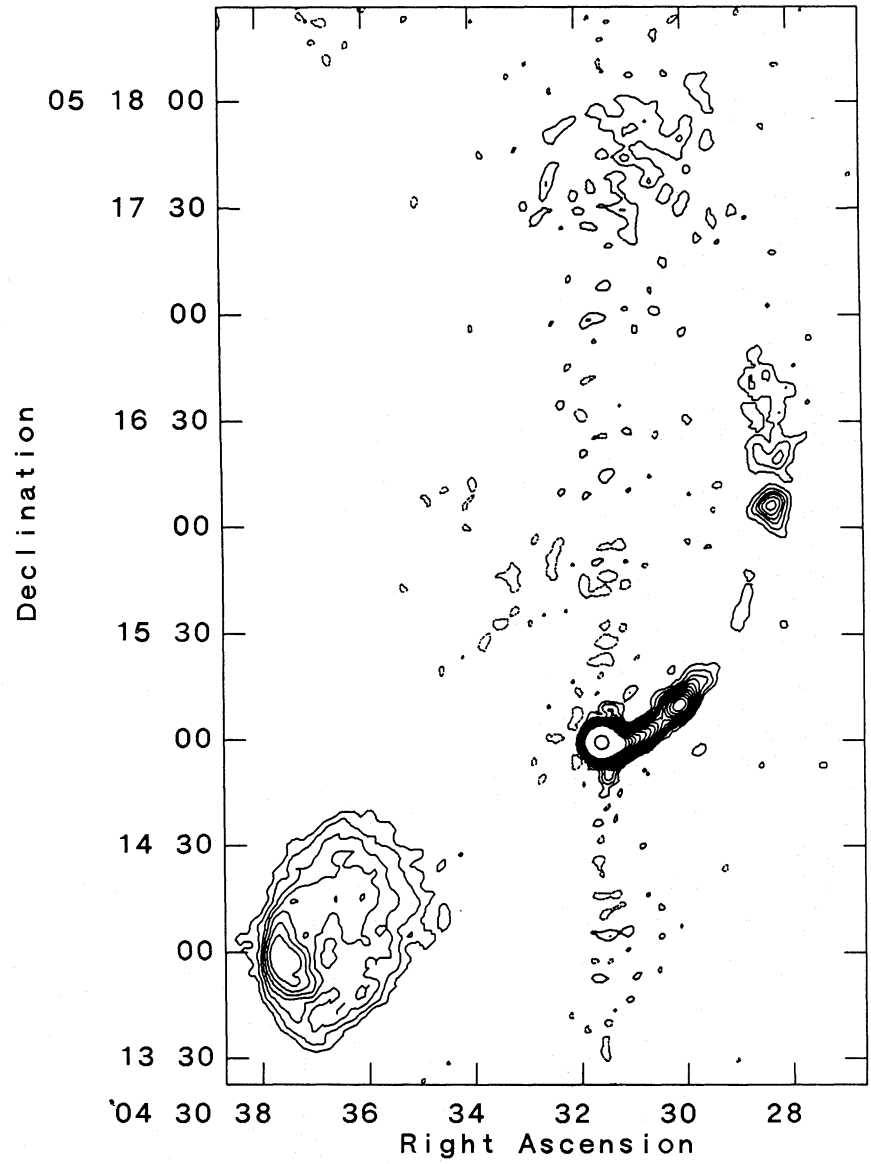

FIG. 9.—The VLA map made with 1.6 GHz data taken with the B-configuration in 1982 October. The convolving beam is nearly circular with a FWHM of 3.″84. The contour levels have been scaled by a spectral index of −0.65 from those in Fig. 8, except that an additional low contour has been added to bring out weak features. The levels are −1.00, −0.60, −0.30, 0.30, 0.60, 1.00, 1.39, 1.93, 2.68, 3.73, 5.18, 7.20, 10.0, 13.9, 19.3, 26.8, 37.3, 51.8, 72.0, and 1820 mJy per beam, and the peak flux density in the map is 3.65 Jy per beam.

tempting to look for a situation, such as is found in Minkowski's object (van Breugel *et al.* 1985), where a burst of star formation is caused by the jet. However, preliminary optical results indicate that the galaxy is a normal spiral with a redshift that is larger than that of 3C 120 by several thousand km s^{-1} (W. van Breugel, private communication). It would seem that this is likely to be a chance superposition (although see Arp 1986).

e) The Lowest Resolution Map

The lowest resolution map available, made from 1.4 GHz, D-configuration data, is shown in Figure 13. The resolution is 37.″5. Several new features are seen at this resolution. The jet, or at least the diffuse structures in the jet direction, is seen to continue for another 2′ or so to the northeast from its previous apparent end. Also, it is now obvious that the whole region inside the bend of the jet, to the north of the core, is filled in with low-level emission (the emission in that area in this map is heavily resolved, confirming the higher resolution results mentioned earlier based on C-configuration, 1.6 GHz data). In addition, there is extended, low-level emission to the southwest of the core. This emission covers an area of over 4′ by 6′ and is brightest in a 2′ "curtain" adjacent to the core and in a diffuse area farther out to the west-southwest. A ridge of emission (note that the word "jet" is not used) extends about 4′ south from the core and then west along the edge of the diffuse emission. These regions do not obviously fit in with the rest of the structure of the source—the three-dimensional geometry is not at all clear. The brightest region about 5′ west-southwest of the core was seen by de Bruyn and Schilizzi (1984), but the weaker and more diffuse emission was either resolved out or below the noise in their observations. The total extent of the

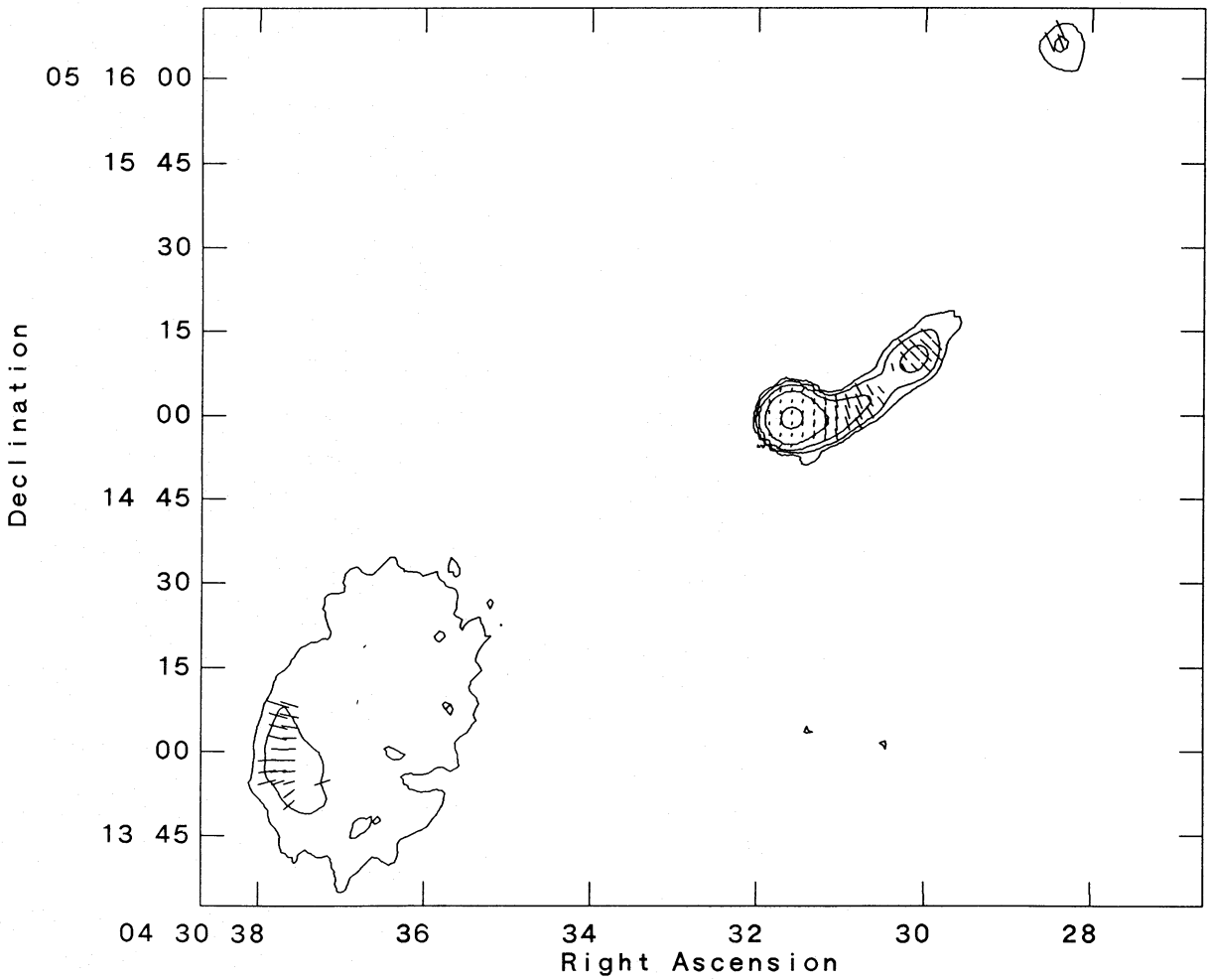

FIG. 10.—The same map as Fig. 8 except that polarization vectors are shown. The polarization vectors are scaled so that a 1″ vector corresponds to 10% polarization. The contour levels are −0.4, 0.4, 1.2, 4.8, 40, and 1014 mJy per beam.

source is about 14′ which corresponds to slightly over 400 kpc in projection.

The polarization structure at the lowest resolution is shown in Figure 14. The field is longitudinal along the jet as seen at lower resolution. In the more diffuse regions, the field shows a vaguely circumferential character and the polarization percentage seems to be rather variable. However, the signal-to-noise ratio is not high enough to show much detail, and no information on Faraday rotation is available.

The large-scale morphology of 3C 120 is rather bizarre. How do the structures to the south-west relate to the rest of the source? The presence of superluminal motions in the core is strong evidence that the inner jet is close (within about 25°) to the line of sight. If so, bends can be exaggerated significantly by projection effects, and strange structures could be the result of looking at reasonably normal lobe structures end-on. A perusal of the radio maps of cluster sources in O'Dea and Owen (1985) or large, weak sources in Ekers *et al.* (1981), trying to imagine what they would look like seen along the axis of the jet, shows that the structures in 3C 120 might not be all that strange. However, note that the projected size of 3C 120 is already 400 kpc so, if it is basically linear and is being viewed end-on, it is very large indeed. It would not be outside the size range of known sources unless the projection factors are very large (3C 236 is nearly 3 Mpc in size for $H_0 = 100$ [Willis, Strom, and Wilson 1974]), but if too many of the sources expected to be viewed end-on are on the outer envelope of the size distribution, something could be wrong with the assumptions (Schilizzi and de Bruyn 1983).

IV. DISCUSSION

The data presented in this paper, along with those from Papers I and II, provide a unique opportunity to study the properties of a radio jet over a very wide range of scale sizes. Nearly the entire range that could be observed in the radio portion of the spectrum is covered. On much smaller scales, the jet becomes optically thick at centimeter wavelengths, and it is likely that structures closer to the core are obscured. A VLBI observation has been done at 22 GHz (not yet reduced) that will have 4 times the resolution of the highest resolution map shown here, but any order-of-magnitude increases in resolution will require the use of much higher frequencies or a VLBI station in space. At the low-resolution end, the jet has been observed out to where it seems to break up, or at least becomes very disturbed. It is not certain that the very largest scale structures in the source have been seen, but there is no evidence in the maps presented here or in the literature for larger structures. In addition to the wide range of scales, infor-

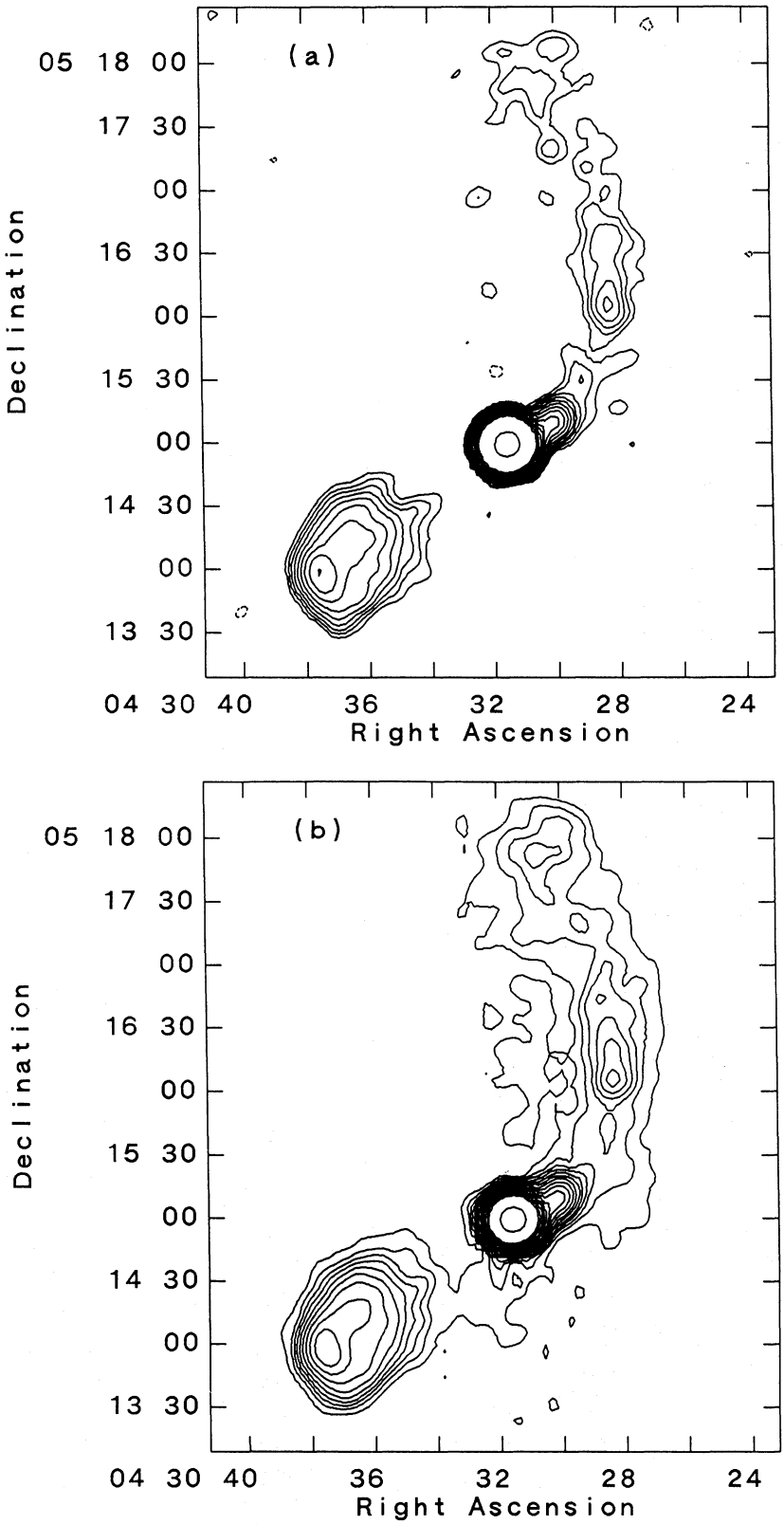

FIG. 11.—Two maps at different frequencies with a resolution of about 11″.8 (FWHM of convolving beam). The contour levels are scaled by a spectral index of −0.65 except one extra low contour has been added to the 1.6 GHz map, and the highest contour in each map is at the half-power point of the peak. (*a*) Map made with 5 GHz data taken with the D-configuration in 1982 December. The contour levels are −1.32, −0.88, 0.88, 1.32, 1.83, 2.54, 3.53, 4.90, 6.81, 9.47, 13.1, 18.3, 25.4, 35.3, 49.0, 68.1, 94.7, and 1404 mJy per beam, and the peak flux density in the map is 2.81 Jy per beam. The map has been corrected for the primary beam of the VLA antennas. (*b*) Map made with 1.6 GHz data taken with the C-configuration in 1984 April. The contour levels are −2.70, −1.80, −0.90, 0.90, 1.80, 2.70, 3.73, 5.18, 7.20, 10.0, 13.9, 19.3, 26.8, 37.3, 51.8, 71.0, 100, 139, 193, and 1144 mJy per beam, and the peak flux density in the map is 2.29 Jy per beam.

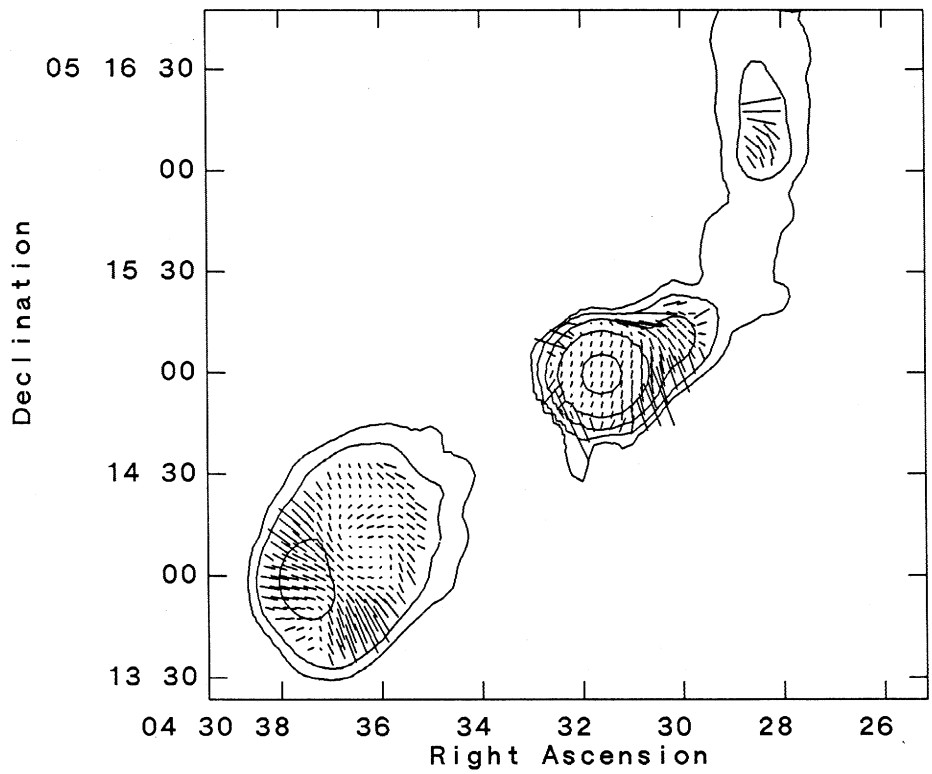

FIG. 12.—The central region of the same map as Fig. 11*b* but with the polarization vectors displayed. The polarization vectors are scaled so that a 10″ vector corresponds to 42% polarization. The contour levels are −2, 2, 4, 16, 100, and 1143 mJy per beam. Again, and especially in this map, the low-flux density regions near the core have unreliable polarization measurements and would not have been displayed except that a uniform cutoff level was used for the display of polarization and a low level is justified in the regions farther from the core. No attempt has been made to remove Faraday polarization but it is probably small. No other polarization data are available at this resolution but comparison with Fig. 10 suggests that any rotation is small.

mation is available from the observed superluminal motions about acitivity near the nucleus of 3C 120 that is only available for a handful of sources, all of which are farther away.

A striking result of these observations is that the 3C 120 jet maintains its character as a well-collimated entity from the inner parsec where motions are seen to scales of about 100 kpc, well outside the parent galaxy. There are no obvious regions where it dissipates and is then recollimated. It seems that the basic characteristics are established within the first parsec and are maintained during at least five orders of magnitude in distance. It is shown below that a closer look at the physical parameters of the jet reinforces the conclusion that it is a coherent entity over the full range of scale sizes.

a) Measured Jet Properties

In order to derive the physically interesting parameters of the jet, an AIPS run file and some special software were developed to make automatically many slices across the jet. A single Gaussian was fitted to each slice to derive the peak and integrated intensities, the position of the peak, and the full width at half-maximum (FWHM) of the jet at the position of the slice. The results were deconvolved from the map-restoring beam. Spot checks of the accuracy of the fits were made but not all of the hundreds of fits were examined individually. Any points that seemed discrepant were checked. The major results to be discussed below are very insensitive to minor errors in any of the fits because of the many orders of magnitude involved.

The flux density per unit length of jet, derived by integrating the emission in each slice across the jet, is shown as a function of distance from the core in Figure 15 on a log-log scale. Data from all maps presented in this paper, except the lowest resolution one, are included. Data from portions of the jet less than two beamwidths from the core are excluded to avoid contamination by the core. All intensities have been adjusted by a spectral index, $\alpha = -0.65$, to correspond to the intensity at 5 GHz. This adjustment is by a factor of about 0.44 for 1.4 GHz and 2.0 for 15 GHz data, so the changes are small compared to the overall range of the data. The highest resolution map was made at 5 GHz so no scaling was done on the most compact structures where the spectral index is most uncertain. The distance from the core is measured directly from the core to the position of the peak in the slice. The distance measured along the jet might be more interesting but harder to define and measure. The difference between the two measures is small compared to the overall range. It is also small compared to the projection effects that the superluminal motions indicate are present.

The region of poor coverage between 100 and 1000 pc from the core is the sparesely covered region between the resolutions of the VLBI and VLA results. The data to be presented in Paper II should provide denser coverage in this region.

The overall behavior of the data can be approximated by a power law. The line through the points represents a power law with an index of -1.27 ± 0.034 that fits the data in a least-squares sense. Deviations from the power law, in the form of excess flux density, are seen on the smallest scales where the superluminal motions are observed, at the locations of the knots seen on the maps, and on the largest scales where the jet is disturbed. On the smallest scales, the source is highly variable so, while these data were taken during a period of low flux

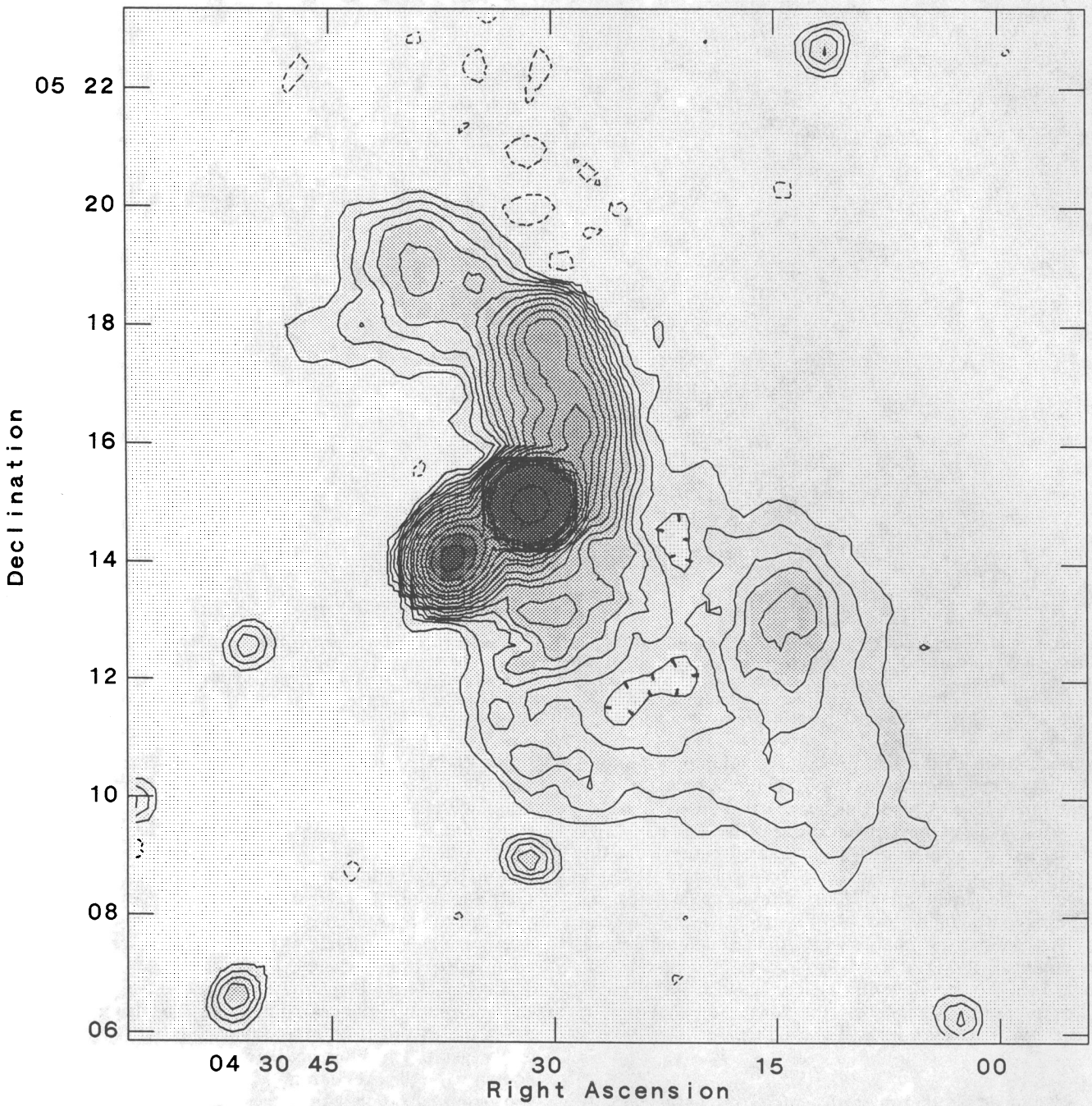

FIG. 13.—The lowest resolution VLA map of 3C 120. The convolving beam has a FWHM of 37".5 and is nearly circular. The map was made from 1.4 GHz, D-configuration data taken in 1984 October. The contour levels are −1.90, −1.20, −0.60, 0.60, 1.20, 1.90, 2.68, 3.73, 5.18, 7.20, 10.0, 13.9, 19.3, 26.8, 37.3, 51.8, 72.0, 100, 139, and 1210 mJy per beam, and the peak in the map is 2.42 Jy per beam. The map has been corrected for the primary beam of the VLA antennas. The small sources not connected with 3C 120 are probably unrelated background objects.

density relative to the previous 20 years, the long-term average flux density from the core region is not known. Also, the standard model for superluminal motions predicts that the emission will be boosted by relativistic beaming by an amount that is rather sensitive to the bulk Lorentz factor, γ, and to the angle to the line of sight. Therefore the observed deviations by about a factor of 3 are actually remarkably small and suggest that there is good continuity of physical parameters along the inner regions of the jet. The brightenings at the knots are discussed below where the brightness is related to the jet width. On the largest scales, the overall morphology is confused, but it is probable that the jet overlaps in projection, if not in space, structures that are not part of the jet proper. This would lead to the excess flux density apparent in the plot.

The value of having such a wide range of scale sizes is clear in Figure 15. Most previous work on jets has had data only over one or two orders of magnitude in scale size. It is clear that the amplitude fluctuations in Figure 15 are sufficiently high that the simple power-law relation would not be seen without several orders of magnitude in distance. On more

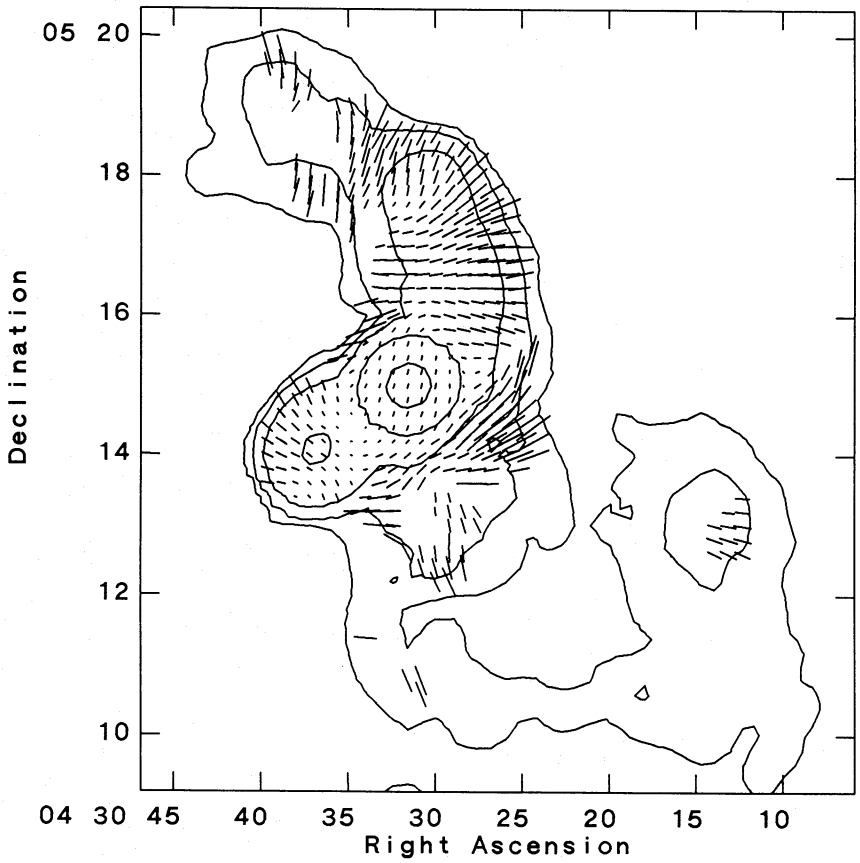

FIG. 14.—The same map as Fig. 13 except showing the polarization vectors. The polarization vectors are scaled so that a 30″ vector represents 45% polarization. The contour levels are −1.2, 1.2, 3, 10, 100, and 1210 mJy per beam. Most of the polarization vectors, except possibility a few about 1′ to the northeast of the core, appear to be reliable. It seems that the curtain of emission southwest of the core is highly polarized. This structure is likely to be a lobe seen in projection against the core.

restricted scales, fluctuations in jet brightness at knots, etc., are the dominant features and tend to be the focus of study. While such features are clues to the details of the jet propagation, they hide the very simple global properties apparent in the 3C 120 data. The wide range of scales also makes the results very insensitive to any measurement errors. Errors of a factor of 2, which are unlikely, would have insignificant effects on the interpretation.

The flux density per arcsecond is displayed in Figure 15 because it is a quantity that is not sensitive to the quality of the measurement of the width of the jet. Similarly, the distance from the core is used rather than the width for the same reason. Unfortunately, derivation of the physical parameters of the jet requires knowledge of the volume of the emission region. This requires measurement of the jet width along with assumptions about the filling factor, the cross-sectional shape of the jet, and the angle of the jet to the line of sight. On most of the maps presented in this paper, the jet is barely resolved in the transverse direction over a significant fraction of its length. As a result, only a fraction of the data can be used for any analysis that requires a volume measurement.

The ratio of the width of the jet (fitted FWHM) to the core distance is displayed as a function of core distance in Figure 16. Only points for which the fitted width of the profile was greater than the beamwidth plus the expected error in the fit width were included. The expected error was determined by first estimating the amplitude error to be the quadratic sum of the off-source rms noise level of the map and 5% of the peak brightness of the profile (10% for the VLBI maps). The percentage errors are estimates of the reliability of the relative amplitudes of features in a map. They are based on experience with tests of mapping procedures and on comparison of the two 5 GHz, C-configuration maps discussed earlier. Note that the probable errors in both the absolute and relative amplitudes of features in a map are much greater than the off-source rms noise level. Once the amplitude error for a slice fit was determined, the width measurement was assumed to have the same signal-to-noise ratio. Resolved points closer to the core than 0.″01, nearly all from the 5 GHz VLBI map, were excluded on the grounds that width measurements from that map are unreliable because of the highly elongated beam. Also points with widths greater than 20″ were excluded to avoid confusion with possible lobe structures.

Note that the ratio of jet width to core distance is larger on scales of tens of parsecs than on kiloparsec and larger scales. This could be the result of either an actual decrease in the opening angle of the jet with core distance or of projection effects in a geometry where the jet is closer to the line of sight on small scales than on large scales. The former case would imply that the confining mechanism is becoming more effective with distance along the jet.

Figure 17 displays the peak intensity, again scaled to 5 GHz, as a function of jet width. A power-law fit to the peak intensity data is shown as a solid line. The index is -2.40 ± 0.08. Note

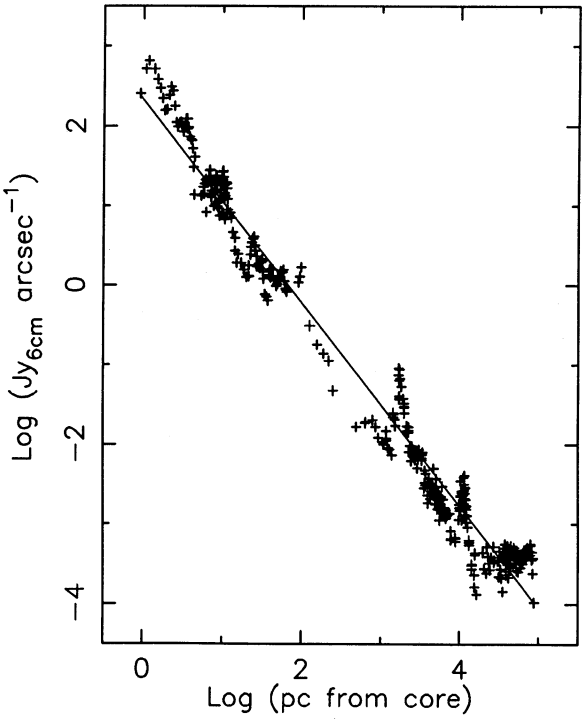

FIG. 15.—Plot of the emission per arcsecond of the 3C 120 jet as a function of the distance from the core. The data are derived from Gaussian fits to slices across the jet. The points represent the integrated flux density in each slice, adjusted for the width of the beam along the jet. This distance is measured directly between the position of the peak on each slice and the core. The line represents a least squares fit and has a slope of -1.27 ± 0.034. The plus signs marking the data points in this and the following figures are not intended to be error bars.

that the power law is a very good approximation of the data over the range for which width measurements are available. That range is about 3.5 orders of magnitude in the width. A power law is a considerably better approximation to the peak intensity vs. width data than to the flux density per unit length vs. core distance data shown in Figure 15. Partly this is because the discrepant data on the largest and smallest scales were eliminated. However, it is also clear that the intensity enhancements at the knots are much less apparent when plotted against width—the fitted FWHM of the jet gets smaller at the location of the knots. This narrowing could be caused either by an actual narrowing of the jet or by the presence of a small, bright region within the jet that leads to a smaller fitted width in a jet whose outer boundary does not actually narrow. The brightness increase would be the natural consequence of any compression of the jet material and would be exaggerated if, as seems likely, shocks formed in the compression region. Brightness enhancements in a relativistic jet also could be created if the velocity of some of the jet material either moved closer to the line of sight or increased in magnitude. The simple relationship between brightness and width suggests that these latter effects do not dominate the overall brightness.

b) Physical Parameters

The power-law relationship between central intensity and jet width suggests that the physical parameters also follow simple power laws. With the information available in these observations, the physical parameters can only be derived by making the usual minimum-energy (or equipartition) assumptions

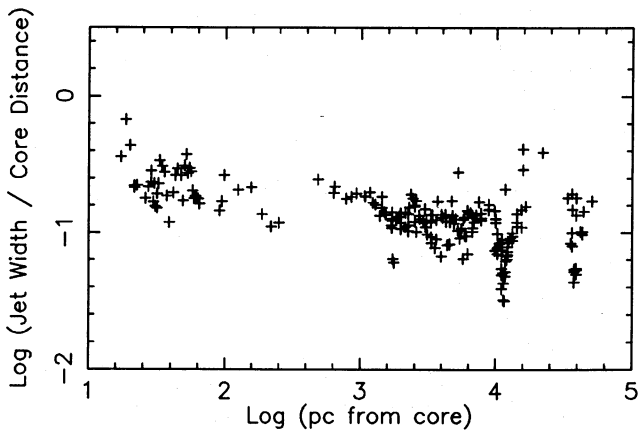

FIG. 16.—The ratio of jet width to core distance as a function of core distance. Only data for which the width measurement is thought to be reliable are included.

(Pacholczyk 1970). The data give the width of the jet and the intensity of the radiation at some frequency as a function of position along the jet. The intensity is converted into a luminosity per unit volume using the assumptions that (*a*) the line of sight through the jet is equal to the width (no attempt is made

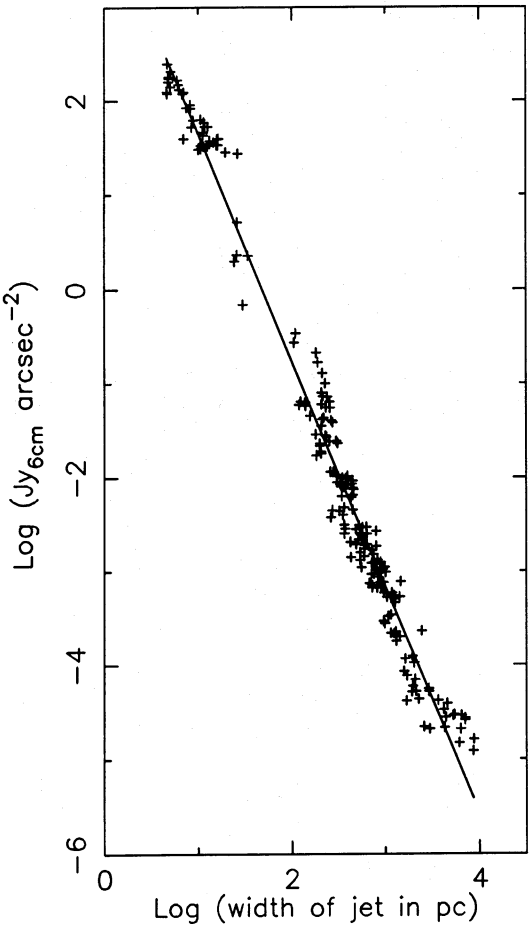

FIG. 17.—The central intensity of the 3C 120 jet as a function of width. The data are for those points, shown in Fig. 16, whose width measurements seem to be reliable. The line represents a least squares fit and has a slope of -2.40 ± 0.08.

to account for projection effects), (*b*) the filling factor of the emitting regions is unity, (*c*) the emission spectrum extends from 10^7 to 10^{11} Hz, (*d*) the spectral index is equal to -0.65 throughout the range of frequencies and throughout the jet, and (*e*) the jet is not relativistic. The luminosity is then used to derive the energy density and other physical parameters under the assumptions that the radiation is produced by the incoherent synchrotron mechanism, that there is equal energy in the radiating particles (electrons) and heavy particles (protons), that the total energy density is divided between particles and magnetic fields in such a way that the total energy density is the minimum that can produce the observed radiation, and that the angle between the magnetic field and the line of sight is 90°.

The above assumptions are those usually used for such calculations. However, as the magnetic field decreases with distance from the core, as discussed below, the assumed frequency range corresponds to an increasing energy range for the particles. But the particles might be expected to lose, rather than gain, energy. Even in the presence of reacceleration, it seems unlikely that the energy range of the particles would move up. To adjust the frequency integration range with position along the jet requires information about the energy losses of the particles or measurements of the broad-band spectra that we do not have. If an integration range were used that slides down in frequency, the luminosity computed from the intensity would decrease somewhat faster than given above. The peak of the emission from a particle of a given energy is proportional to the magnetic field. If the magnetic field decreases with the inverse of the jet radius, as suggested below, and the electrons maintain constant energy, the integration limits that should be used would move down with the inverse of the jet radius. The luminosity is roughly proportional to the integration limits to the $(1 + \alpha)$ power. The minimum energy density, in turn, is proportional to the luminosity to the $\frac{4}{7}$ power and therefore is proportional roughly to the integration limits to the 0.2 power for $\alpha = -0.65$ (for this spectral index, the sensitivity is mostly to the upper integration limit). Therefore, in this scenario, the powers of the dependencies of the minimum energy density and magnetic field on radius would be decreased by 0.2 and 0.1, respectively. This is not a strong effect. The argument is somewhat circular since the dependence between the radius and the integration limits depends on the magnetic field result obtained assuming no change in integration limits. However, the dependence is so weak that the circularity does not matter.

Another problem with the above assumptions is that they apply to a nonrelativistic source. However, the superluminal motions observed near the nucleus imply that at least part of the source is relativistic and near the line of sight. The observed motions of $v/c \approx 4$ imply that relativistic beaming has boosted the intensity of the observed radiation by a factor in the range of 10–100, depending on the angle to the line of sight. The luminosity per unit volume of the source, in the regions of relativistic motion, is lower than that given below by a similar factor. The luminosity is also affected by additional factors resulting from projection effects and from changes in the limits of integration, but those factors are smaller than the uncertainty in the amount of beaming. Note that, if the intensity is boosted by a factor near 10 in the inner few parsecs and the rest of the jet is unbeamed, the correlation shown in Figure 15 is improved while the slope is decreased somewhat. This amount of beaming is expected for angles to the line of sight in about the outer half of the allowed range ($\sim 12°$ to 24°). Such angles to the line of sight are favored by solid angle considerations. They also help minimize the difference between the true size and the already very large projected size of the overall source. However, observational selection effects would tend to favor the brighter sources that have small angles to the line of sight. If the luminosity is overestimated by a factor of 10–100, the minimum energy density will be overestimated by a factor of 4–14 and the magnetic field by a factor of 2–4. Errors of this magnitude alter the quantitative results given below somewhat but do not significantly alter the qualitative conclusions.

A final caveat concerns the assumption that the radiation is produced by the incoherent synchrotron mechanism. This is the usual assumption for extragalactic radio sources. However, some doubt has been expressed based on the observed dominance of coherent emission in laboratory jets and in the solar system (cf. Benford 1984). If the emission mechanism is coherent, directly observed quantities such as the luminosity and Faraday rotation are not affected. However, deduced quantities such as the energy density, pressure, and particle lifetimes could be seriously in error. The fact that the pressure calculated below is in rough balance with expected external pressures is weak evidence in favor of incoherent processes.

The geometry assumed for the calculation of the physical parameters is an optically thin cylinder. The total emission seen in each slice is assumed to come from a disk whose thickness along the jet is 1.064 times the FWHM of the beam along the jet (the area of a Gaussian is its peak amplitude multiplied by 1.064 times its FWHM) and whose diameter is 1.5 times the deconvolved FWHM (r) of the jet along the direction of the slice. The factor 1.5 is approximately the ratio between the diameter of an optically thin cylinder and the FWHM of a Gaussian fitted to the emission profile of that cylinder. This was determined numerically and depends somewhat on the ratio of beam to cylinder size since a Gaussian is not a perfect description of the emission profile of a cylinder.

Under the above assumptions, the emissivity (luminosity per unit volume per steradian) of the jet is

$$\epsilon = \int_{10^7}^{10^{11}} d_l S(\nu_0, r) \left[\frac{2.06 \times 10^5 (1+z)^2}{d_l}\right]^3 \times \left[\frac{1}{\pi(1.5r/2)^2}\right] \left(\frac{\nu}{\nu_0}\right)^{\alpha} d\nu , \quad (1)$$

where d_l is the luminosity distance to the source (3.1×10^{26} cm), $S(\nu_0, r)$ is the flux density received from a unit length of the jet in Jy per arcsecond, the cubed term converts the units of volume from arcseconds to cm, r is the measured FWHM of the jet in arcseconds, ν_0, is the observing frequency, and α is the spectral index. Using the data from Figure 17, the emissivity is

$$\epsilon = 7.3 \times 10^{-26} r^{-3.40} \text{ ergs s}^{-1} \text{ cm}^{-3} \text{ sr}^{-1} . \quad (2)$$

c) *Energy Density and Magnetic Field*

The minimum energy density of a medium with the observed emissivity is proportional to $\epsilon^{4/7}$. Under the assumptions listed above, the minimum energy density in the 3C 120 jet is

$$U_{\min} = 1.5 \times 10^{-10} r^{-1.95} \text{ ergs cm}^{-3} . \quad (3)$$

The calculated minimum energy densities for the 3C 120 data points with good width measurements are shown in Figure 18. The line is a representation of equation (3) (the calculated result based on equation [2] and a fit to the data agree—the

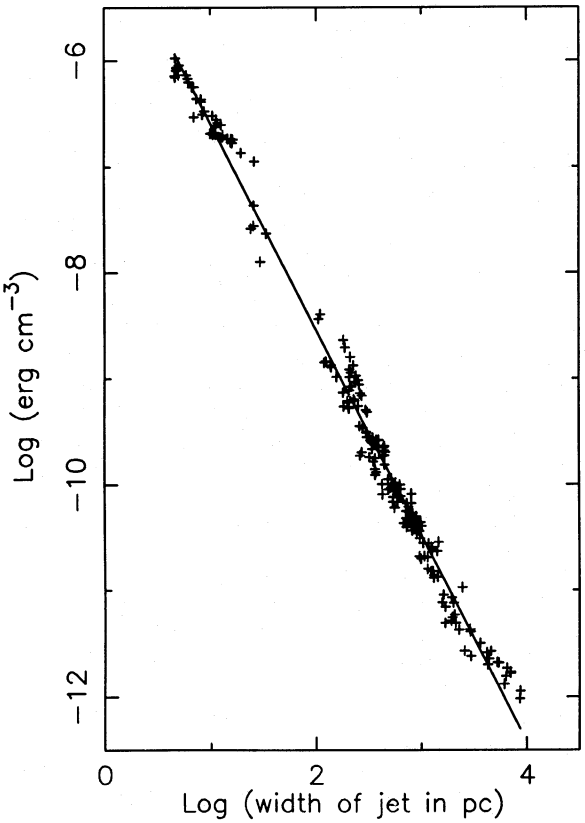

FIG. 18.—The minimum energy density as a function of jet width for the data given in Fig. 17. The line represents a least squares fit to the data and has a slope of -1.95 ± 0.08. Note that for a slope of -2.0, the energy content per unit length of the jet is constant.

same math is used for both). The formal error of the fit to the exponent on r is ± 0.08. Note that an exponent of 2.0 is within the errors. Since the cross-sectional area of the jet increases with r^2, equation (3) implies that the energy content per unit length of the jet is very nearly constant. If the assumptions used to derive this result are approximately correct, either very little energy is being lost as the jet material moves away from the core, or the jet is slowing down just enough, thereby increasing the energy density, to counter any losses that are experienced.

The magnetic field under the minimum-energy assumption is proportional to the square root of the energy density. For 3C 120, it is given by

$$B = 4.1 \times 10^{-5} r^{-0.97} \text{ G} . \quad (4)$$

Thus the magnetic field is inversely proportional to the diameter of the jet, within the errors on the determination of the exponent on r. Although the field was calculated under the assumption that the minimum energy condition is maintained, its variation with r is what might be expected for the flux-conserving expansion of a jet with a transverse magnetic field. However, the polarization data presented earlier show that the field is longitudinal, at least in the region of the dominant emission. A longitudinal field undergoing flux-conserving expansion is expected to decrease with the square of the jet width.

d) Particle Lifetimes

The lifetime of the particles radiating the observed radiation is proportional to $B^{-3/2}\nu^{-1/2}$. The calculated lifetimes, in years, of the observed radiating electrons are shown in Figure 19 as a function of the distance from the core measured in light years (R_{ly}). The frequency used in the calculations was the observing frequency. The core distance is shown in units of light years to aid in interpreting the relationship between the particle lifetimes and the time they might spend traversing the jet. The line on the plot is the result of a fit that indicates that the lifetimes are approximated by $17(R_{\text{ly}})^{1.2}$ years. This result is only approximate because of the use of several frequencies, but it shows that, for jet velocities greater than about 1% of the speed of light (most of the allowed range—see below), the particles do not lose their energy in a distance short compared to the distance back to the central engine. Therefore, the need for acceleration of particles at locations away from the nucleus is not as clear as for some other sources, for example, the hot spots in Cygnus A, where the particle lifetimes are much shorter than the light-travel time back to the nucleus.

However, the need for particle acceleration is not completely gone. While the lifetimes of the observed particles are longer than the light-travel time back to the core by at least two orders of magnitude, those particles were not subject to the same environment near the core as where they are observed. Near the core, the magnetic field is higher, so the particles, having the same energy as those seen farther out, emitted radiation at higher frequencies and had shorter lifetimes. For an example, assume that the magnetic field decreases with the inverse of the jet width, as suggested by the minimum-energy calculations. Then consider particles with the same energy as those observed in the outer regions. When those particles are in the high magnetic fields within a few parsecs of the core, their lifetimes are less than the light-travel time from the core. This situation applies over a much larger region if the rate of decrease of the magnetic field is faster, as would be expected in a flux-conserving, longitudinal field jet. Therefore, particle acceleration away from the core is needed.

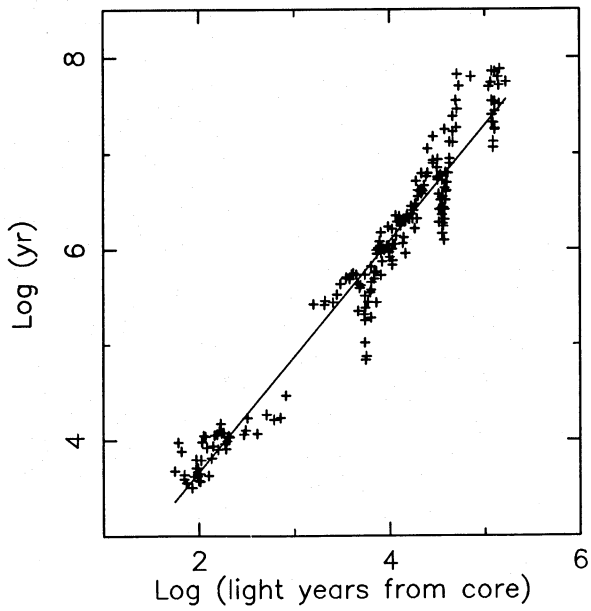

FIG. 19.—The lifetime of the observed emitting electrons as a function of distance from the core in light years. The data are those shown in Fig. 17. Note that the lifetimes are on the order of 100 times the light-transit time from the core.

e) Pressure

The minimum internal pressure due to the relativistic gas in the emitting region is given simply by $\frac{1}{3}U_{\min}$. It is useful to express the pressure in terms of the number density times the temperature that would be required of an external medium to contain the emitting gas by thermal pressure. That is given by

$$nT = 3.7 \times 10^5 r^{-1.95} \text{ cm}^{-3} \text{ deg} . \quad (5)$$

Perhaps more instructive for comparison with expected densities and temperatures is to display the internal jet pressure as a function of distance from the center of the galaxy, assumed to be coincident with the core. Those data are shown in Figure 20. The data have again been restricted to that shown in Figure 16. Since the ratio of jet width to core distance decreases with distance along the jet, the slope of the pressure vs. core distance curve is flatter than the pressure vs. width curve. The index to the power-law fit to the data in Figure 20 is -1.7 ± 0.1, where the error is the formal error of the fit.

How does the calculated minimum pressure of the 3C 120 jet compare with that of the surrounding medium? Unfortunately we do not have good information specific to 3C 120 on the pressure of the interstellar gas, so typical values for active galaxies will have to be used. In a typical broad-line region, confined to the inner few parsecs, the line-emitting gas is thought to have a density of 10^9–10^{10} cm^{-3} and a temperature of about 10^4 K (Osterbrock 1979; Ferland and Shields 1985). The product is therefore 10^{13}–10^{14}, well above the values for the 3C 120 jet. Either the typical pressure in AGN line-emitting clouds does not apply throughout the inner few parsecs, or 3C 120 is not typical, or the pressure in the jet is well above the minimum value.

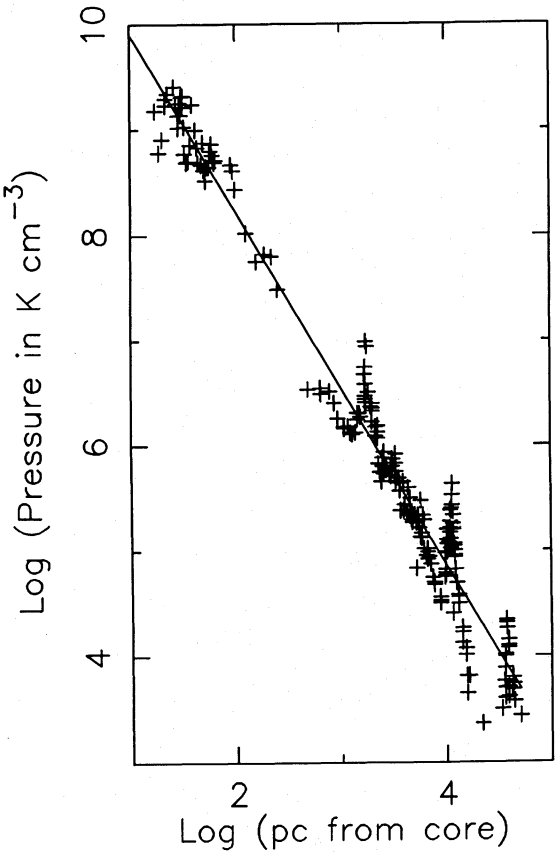

FIG. 20.—The internal pressure of the 3C 120 jet, calculated under the minimum-energy assumption, as a function of distance from the core. The pressure is displayed in units of the product of the external density and temperature that would be required for pressure balance. The center of the galaxy can reasonably be assumed to be coincident with the core so the data can be used to compare pressures with conditions that might be expected at various locations from the inner few parsecs to outside the galaxy. The line represents a power-law fit and has a slope of -1.67 ± 0.07. The data have been restricted to the same set with good width measurements as shown in Fig. 17.

Typical narrow-line clouds are in the range 100–1000 parsecs from the nucleus and are thought to have densities of 10^3–10^5 cm^{-3} and a temperature again of 10^4 K (Osterbrock 1979; Ferland and Shields 1985). That gives a density-temperature product of 10^7–10^{10}. At that projected distance from the core, the 3C 120 pressure is just below this range. The imbalance noted for the broad-line region still exists, but is probably not very significant compared to the errors on all the numbers involved. Also, if the jet is near the line of sight as implied by the superluminal motions, the error in the apparent core distance is in the right sense to alleviate the imbalance.

In the disks and coronae of spiral galaxies such as our own, the density-temperature product is between 10^3 and 10^4 at distances of 5–10 kpc from the nucleus, although there is a considerable range of densities and temperatures (cf. Spitzer 1978; Myers 1978). X-ray observations of bright, early-type galaxies indicate a similar pressure ($nT \approx 10^4$) at similar distances (Forman, Jones, and Tucker 1985). These values are just below the values calculated for 3C 120. Given the probable errors in the pressure determinations, pressure balance could exist. Farther out, the pressure in the coronae about early-type galaxies appears to decrease with distance at a rate approximately proportional to $R^{-1.5}$ (Forman, Jones, and Tucker 1985). This is not significantly different from the $R^{-1.7}$ rate seen in 3C 120, given the uncertainties in both rates. The coronae can extend to, or beyond, the 100 kpc scales where the 3C 120 jet breaks up. Therefore, it is likely that, if 3C 120 has a corona like those seen in early-type galaxies, the jet is in pressure balance with it and does not survive beyond it. If there is no such corona, the jet is probably overpressured with respect to the intergalactic gas which an interpretation of the X-ray background spectrum suggests has a temperature near 10^8 K and a density of about 10^{-7} cm^{-3} (Fabian and Kembhavi 1982).

Note that the expected external pressure is greater than the minimum internal pressure near the base of the jet and decreases relative to the internal pressure with distance from the core. The maps in this paper show that the jet is initially collimated on subparsec scales and that the collimation is maintained, if not increased, from there on. Since the minimum internal pressure seems to be below the expected external pressure, it is reasonable to suppose that the jet is confined by a smoothly decreasing external pressure and that it expands to maintain pressure balance. The nominal pressure values discussed above allow the jet pressure to be well above the minimum value in the central regions of the galaxy but suggest that it is likely to evolve toward a minimum energy condition as it moves outward.

f) Density

Both thermal plasma and the relativistic gas responsible for the observed radiation could contribute to the jet density. It was shown earlier that there is no significant Faraday rotation in the jet, either on scales above 1″ or in the regions near the

core that dominate the polarized emission from the core in the VLA maps. This fact can be used to set upper limits on the density of thermal plasma in the emitting region under the assumption that the magnetic field is dominated by a uniform, line-of-sight component (cf. Kraus 1966). Using the geometry of an optically thin cylinder where the average path length of emitted photons is $0.59r$, the 3C 120 width data and the upper limit to the Faraday rotation of 0.35 radians at 1.4 GHz give an upper limit to the density of $n \leq 9.9 \times 10^{-4} r^{-0.03}$ cm^{-3}. This is very nearly a constant upper limit to the density of thermal gas of 10^{-3} cm^{-3}. Since the total flux density is dominated by regions less than 10 pc from the core as shown by the VLBI maps, it is likely that the polarized emission in the core on the VLA maps is also dominated by features less than 10 pc from the core implying that, even on these scales, the density of thermal gas is less than 10^{-3} cm^{-3}. If there are field reversals along the line of sight, it is possible to have higher densities with no net Faraday rotation. However, if there are significantly higher densities, depolarization would be expected in some such cases but is not seen.

The number density of radiating particles in the relativistic gas responsible for the emission is proportional to the luminosity over the magnetic field. Using the values derived for 3C 120 above, that number density is about $6.7 \times 10^{-8} r^{-2.43}$ and is rather sensitive to the lower integration limit used in the luminosity calculation. Note that this number density decreases faster than the volume of the jet increases. This is an artifact of use of integration limits based on observing frequency. As the magnetic field decreases, the limiting frequencies correspond to higher energies. If more realistic integration limits that slide down in frequency along the jet were used, the number density would decrease more slowly, but a detailed calculation requires more information than is available.

The above equation gives a density of radiating particles near 0.2 cm^{-3} when the jet width (FWHM) is 1 pc (several pc from the core). This is well above the limit set by Faraday rotation for thermal electrons. However, the Faraday rotation caused by relativistic particles is reduced by γ^2 (Wardle 1977) so the higher density does not violate the Faraday rotation limits. Here γ is the Lorentz factor of the individual relativistic particles, not the bulk motion. If the radiating particles are electrons in charge balance with protons, the above result, along with the upper limit to the thermal density, implies that the mass of the jet on scales of a few parsecs is dominated by the protons associated with the relativistic electrons. Thermal material is relatively unimportant. This conclusion is not firm because the use of a higher low-frequency cutoff, combined with accounting for beaming effects that are likely to be present, can lower the derived density of relativistic particles to below the limit on thermal particles. Future high-resolution, multifrequency, polarization VLBI observations, perhaps with the VLBA., could put the conclusion on a firmer footing. For now, the data suggest only that the thermal material is not an important component of the jet on small scales. Of course, the mass density of the emitting gas could be much lower, and no Faraday rotation would be seen, if charge balance were provided by positrons as expected for some electromagnetic jet acceleration mechanisms (cf. Begelman, Blandford, and Rees 1984).

g) Adiabatic Expansions

The constancy of the energy per unit length derived above is consistent with a jet that travels at constant velocity and suffers no significant energy losses. However, it is also possible to obtain the same result in the presence of energy losses if the jet is slowing down and/or if the jet is not in the minimum energy condition. It is instructive to compare the observed intensity decrease with that expected for an adiabatically expanding jet with a variable velocity. In the simple case of adiabatic expansion with magnetic flux conservation, the central intensity of a jet with a -0.65 spectral index is expected to decrease as $r^{-5.2}$ $v^{-1.4}$ in the case of a longitudinal magnetic field or as $r^{-3.5}$ $v^{-3.1}$ in the case of a transverse magnetic field (Bridle and Perley 1984). Here v is the flow velocity of the jet. For the observed intensity decrease, $I \propto r^{-2.40}$, the velocity would be proportional to $r^{-2.0}$ in the longitudinal case and proportional to $r^{-0.35}$ in the transverse case.

If the velocity is near 10^5 km s^{-1} near the core (an arbitrary value near c), by the time a jet with a longitudinal field reaches the lobes, it is traveling at only a few centimeters per second. At such velocities it takes about a Hubble time to travel a parsec and there are over 100 kpc to traverse. Therefore the simple longitudinal case seems unlikely. However, the much slower decrease of velocity for the transverse case cannot obviously be ruled out with such arguments, but that case requires an explanation of why the observed field appears to be longitudinal.

h) Velocity Constraints

There is no direct evidence in any extragalactic jets that gives the fundamental physical parameters of velocity and density. Any studies of the physics of jets either have to assume values for these parameters or have to explore the parameter space of possible values. This is not a very satisfactory situation. The best evidence for specific velocities are the superluminal motions observed in some powerful, one-sided sources near the core and constraints imposed by two-sided symmetry of weak sources (Bridle and Perley 1984). The standard model for superluminal motions (cf. Blandford and Königl 1979) requires relativistic velocities in the first few parsecs of the jets in which they are observed. On the other hand, the weak, two-sided sources are almost certainly not relativisitic. This is especially true of the head-tail sources where bending obviously occurs but no beaming effects are seen. There is no convincing evidence for the velocity of the weak jets near the core or for the powerful jets at kiloparsec distances. It is tempting to explain the one-sidedness of the powerful sources as a beaming effect in a relativistic source, but such attempts tend to run afoul of statistics—among other problems, one-sided sources are too common in samples that are not expected to have an orientation bias (cf. Wardle and Potash 1984).

Because it is a superluminal source and has large-scale, bent structure, 3C 120 is an interesting source in this discussion. However, there appears to be insufficient information still to settle the question of the velocity of the large-scale jet. Nevertheless, it is instructive to consider some of the possible constraints on the velocity.

A crude, but firm, lower lomit of roughly 20 km s^{-1} can be placed on the jet velocity by the necessity to get the material to the outer lobes in less than a Hubble time. This necessity also constrains the velocity to decrease slower than about r^{-1}, even if it starts out near the speed of light. As mentioned earlier, this excludes a longitudinal-field, flux-conserving, adiabatic expansion.

More interesting constraints are obtained by considering the need to transport enough energy to the outer regions of the source to provide the emission that is seen (cf. Bridle and

Perley 1984). To do this, it is necessary to assume that the current energy transport is the same as that in the past so that the current large-scale emission, times some efficiency factor, can be equated to the energy flux in the jet. Two possibilities will be considered. The first applies to a jet in which most of the energy transport is in the form of bulk kinetic energy. The second possibility is that the energy transport is dominated by the convection of the internal energy associated with the relativistic particles and magnetic fields responsible for the radio emission. The results of these calculations cannot provide more than a very rough estimate of, or limit on, the velocity because of the large uncertainties in the input data and the assumptions, especially the implied assumptions that the source is not growing and that the energy transport in the jet has remained roughly constant over its life. Note that, if the source is growing, or if the jet carries more energy now than in the past, the velocity will be underestimated. For simplicity, the nonrelativistic equations will be used with the understanding that, if the resulting velocity is near or above c, the large-scale jet is constrained to be relativistic.

The velocity in the case dominated by bulk kinetic energy is given by

$$v_j = \left[\frac{2L_{\rm rad}}{\eta A_j \rho_j}\right]^{1/3}, \quad (6)$$

where v_j is the jet velocity, $L_{\rm rad}$ is the radiation emitted in regions beyond the point of interest in the jet, η is the efficiency of conversion of kinetic energy to radiated energy, ρ_j is the jet density, and A_j is the area of the jet. Losses of energy to anything other than radiation are accounted for in the efficiency term.

The total luminosity of the large-scale structures, which are unlikely to be subject to beaming, is roughly $5 \times 10^{10}(4\pi d_l^2)$ times the 5 GHz flux density, assuming that the spectral index is -1 and the limits of integration are 10^7–10^{11} Hz. A conservative estimate (i.e., low) of one-half of the 5 GHz flux density from regions outside the jet is about 0.025 Jy. One-half was used to allow for the possibility of a counterjet. With these numbers, the luminosity of the lobes powered by one jet is about 1.4×10^{40} ergs s^{-1}. An upper limit to the density of thermal material of about 10^{-3} cm^{-3} was derived above from the Faraday rotation measurements. Assuming that $\eta = 1$, the jet velocity is greater than $1.7 \times 10^3\, r^{-2/3}$ km s^{-1}, where r is, as before, the measured FWHM of the jet in arcseconds. A lower efficiency or density would give a higher velocity but the dependence is relatively weak thanks to the $\frac{1}{3}$ exponent.

This argument suggests that, if the energy transport is dominated by bulk kinetic energy, the velocity is greater than $0.01c$ where the jet diameter is just over 0.″5 and could be significantly greater if the efficiency and density used above are too high as seems likely. The same argument applied in the first few parsecs gives a higher velocity, but, if protons provide change balance and are as dense as suggested earlier (0.2 cm^{-3}), the velocity is still not relativistic. Therefore this argument cannot constrain the jet to be relativistic, even on small scales, unless stricter limits can be determined for the efficiency and/or density.

Energy is also transported along the jet by convection of the internal energy of the radiating gas. More properly, the enthalpy should be considered but the difference is a factor of order unity and will be ignored here. The minimum energy per unit length in the 3C 120 jet, based on the minimum energy density calculated above, is very close to 10^{33} ergs cm^{-1} throughout the length of the jet. If that energy is to power the lobes by being convected out to them, the velocity must be above about $1500/\eta$ km s^{-1} ($0.005\, c/\eta$), not taking into account adiabatic losses. Note that this estimate depends inversely on the efficiency, rather than on $\eta^{-1/3}$ as for the bulk kinetic energy case, so any loss of efficiency quickly drives up the velocity. However, the energy is already in the desired form so the efficiency could be high.

These arguments show that it is possible to power the lobes with bulk kinetic energy or convected internal energy in a nonrelativistic jet. Jet velocities above a few thousand km s^{-1} are consistent with current constraints on the density and efficiency. If arguments or data can be found that constrain the density and/or efficiency to be lower than the values used here, it may become possible to use these arguments to constrain the jet to be relativistic, but for now that is not possible.

The one-sidedness of the visible structure provides a lower limit to the velocity of the jet under the assumption that the one-sidedness is due to relativistic beaming. However, that is not the only possible cause of one-sidedness. It could be due to some difference between the characteristics of the jet and the counterjet that cause the counterjet to emit less radiation. Or it could be due to intrinsic one-sidedness. The southeast lobe is evidence that a counterjet either exists or did exist at one time. If the jet is intrinsically one-sided, it must have reversed direction at some time (for "flip-flop" models, see Rudnick and Edgar 1984), although there is no obvious corresponding gap on the jet side.

No evidence of a counterjet closer to the core than the southeast lobe is seen in any of the maps. However, the high brightness of the core relative to the jet, along with finite dynamic range, limits the sidedness ratio limits that can be set. Several maps show the lack of any feature east of the core that is equivalent to the 4″ knot at a sidedness ratio of about 100:1. The 5 GHz, VLBI map also shows a sidedness ratio of about 100:1 between the brighter superluminal features and the highest noise bump on the other side of the core. The highest sidedness ratio measured is about 200:1 in the 1.6 GHz, B-configuration map at about 8″ from the core (comparing the flux density per beam of the jet at that distance with the highest point in a region of about 1000 square arcseconds immediately to the east of the core). If the one-sidedness is the result of relativistic beaming, a sidedness ratio limit of 200:1 requires that a jet with a spectral index of -0.65 have $\gamma \geq 1.6$, taking into account the increase in brightness of the approaching side and the decrease in brightness of the receding side (Blandford and Königl 1979). This γ is smaller than that implied by the superluminal motions ($\gamma \approx 4$) so the observed sidedness is consistent with a jet velocity on the large scales that is the same as that seen on small scales. A 200:1 sidedness ratio limit, if due to beaming, also constrains the angle to the line of sight on large scales to be less than about 40°, although γ must be above about 4 for that high an angle.

In some systems, it is possible to place upper limits on the jet velocity based on the lack of apparent beaming effects (Bridle and Perley 1984 and references therein). However, for 3C 120, where beaming effects may explain some of the structure, there is no obvious upper limit to the velocity. Certainly the 3C 120 jet cannot be constrained to be nonrelativistic. Extreme relativistic velocities might be excluded by the lack of overwhelming beaming effects (e.g., extreme brightness changes at bends), but it is not clear now to make quantitative limits.

i) Bending

The mechanism responsible for bending of the jet in 3C 120 is not clear. For head-tail sources in clusters of galaxies, ram pressure due to the motion of the parent galaxy through the intracluster medium is the likely mechanism (Begelman, Blandford, and Rees 1984, and references therein). Changes in the direction of the source of the jet is another possible mechanism and, in the form of precession, is the cause of bending in the galactic source SS 433 (Margon 1984). However, for wide-angle tail sources associated with dominant cluster galaxies (cf. Eilek *et al.* 1984), the bending mechanism is not clear. Motions through a cluster medium cannot be invoked for 3C 120 because it is an isolated galaxy. Little is known about the external medium around 3C 120, partly because of the lack of observations of extended X-ray emission in 3C 120. Such observations may be difficult in the presence of the bright X-ray core. About all that can be done here is to discuss the reasonableness of various bending mechanisms.

For ram pressure to be the cause of the bending of a radio jet, there must be relative motion of an external (to the jet) medium across the jet. The force generated must be sufficient to change significantly the momentum of the jet material. Meanwhile, using the same steady-state assumption used in the discussion of jet velocity, the energy flow along the jet must be sufficient to power the emission in regions farther out. Roughly following the analysis of O'Dea (1984) for a high Mach number ("cold") jet, but absorbing the relativistic and adiabatic terms into the efficiency and requiring that the jet power the outer regions of the source, ram-pressure bending requires that

$$\frac{\rho_e v_e^2}{h} = \frac{2L_{\rm rad}}{v_j \eta \pi r_j^2 R} . \quad (7)$$

The left side is the ram-pressure force exerted by the motion of the external medium across the jet on a unit volume of the jet. The quantity ρ_e is the density of the external medium, v_e is the velocity of the external medium across the jet, and h is the scale height over which the pressure is exerted. The right side of the equation is the change of momentum required of the jet with the constraint that the jet power the outer source used to remove the most uncertain parameter, the jet density (although η is also uncertain). The quantity $L_{\rm rad}$ is the radiated energy powered by the jet, η is the efficiency of conversion of bulk energy into radiation including any relativistic and adiabatic corrections, r_j is the jet radius ($0.75r$ where is the FWHM as explained earlier), v_j is the jet velocity, and R is the bending scale length (radius of curvature). This equation cannot be used to place any limits on the ram pressure because we do not have an upper limit to the jet velocity or a lower limit to the efficiency.

Reasonable jet parameters for the bend at about 10″ are a luminosity of 1.4×10^{40} ergs s^{-1}, a jet diameter ($2r_j = 1.5r$) and scale height (h) of 0.″9, and a radius of curvature of 10″. The assumed value of the efficiency η is 0.01 and of the beam velocity is $0.1c$. These values give $\rho_e v_e^2 = 3.3 \times 10^{-11}$ dyn cm^{-2}. The region of the bend is at a projected distance of 5 kpc from the center of the galaxy, although the true distance is likely to be a few times larger because of the projection effects. At such distances, the external medium is likely to be the interstellar medium of the galaxy. The above value of $\rho_e v_e^2$ could be obtained with a density of 0.05 cm^{-3} and a velocity of 200 km s^{-1}. These values are reasonable for an interstellar medium especially considering that there are probable errors of an order of magnitude or more in the assumed jet velocity and efficiency. If projection effects are serious, the region of concern is farther from the center of the galaxy where the density is lower, but the radius of curvature would be larger so the values are probably still reasonable. In summary, it seems that the bend at 10″ could reasonably be the result of ram-pressure bending by normal interstellar gas. A weakness of this scenario is that it will not work if the jet is aligned with the rotation axis of the galaxy as suggested by the measurements of Baldwin *et al.* (1980) and as might be expected for scenarios where the jet is ejected along the rotation axis of an object in the galactic center.

The bending also could be a relic of changes in orientation of the central engine, perhaps due to orbital motions, to precession, or to some less periodic perturbation. Individual elements of the jet could be moving in straight lines but the jet appears bent because of the changing direction of successive elements. A special version of this scenario involves steady precession. The geometry for this case is amenable to computer modeling (cf. Gower *et al.* 1982 and references therein) so we have attempted to fit the observed trajectory of the 3C 120 jet on scales from 1″ to 30″ with such a model. Such models have the problem that, if enough parameters are varied, almost any geometry can be fitted. However, they do have the distinct advantage that they are the explanation for the geometry of the only jet for which the velocity and bending mechanism are known: SS 443 (see Margon 1984). To avoid having too many free parameters, we forced our model to have a constant precession rate and to have a constant bulk velocity, or γ, equal to that implied by the observed superluminal motions. With these constraints, it was impossible to obtain a good fit to the data. This implies that, if precession is the cause of the bending, either the precession rate is not constant, the velocity is not that seen near the core, or the velocity is not constant. Virtually any bending shape could be the result of secular variations in the orientation of the central source so, while such variations may well be the explanation of the observed geometry, it does not seem productive to model those variations in detail without further observational constraints.

Another possible explanation for the bending in an isolated source such as 3C 120 is that it is a manifestation of some instability in the jet propagation (cf. Hardee 1984, and references therein). At least in the linear perturbation regime, such instabilities in jets are likely to occur, although it is not clear if the amplitude can grow enough to cause pronounced bending of the whole jet. Such instabilities naturally account for the observation that in many sources, including 3C 120, the bending radius increases with distance from the core and the direction of curvature does not remain constant. Precessing and ram-pressured bending models have difficulties with these points.

As noted before, the mechanism causing bending in 3C 120 is not clear. It is likely that any of the above mechanisms could work. The brightness enhancement on the outside of the bend at about 10″ suggests that some interaction with the external medium is occurring at the bend so a ram-pressure model may be correct. However, it is possible that such a structure would occur in an unstable jet or in one subject to variations in the initial direction. In both cases, the outside of the bend is where jet material is interacting with external material rather than flowing down the previously opened channel. Note that the edge brightening would be seen only for bends in planes across the line of sight. Therefore the confined region of edge bright-

ening does not exclude situations where bending is occurring all along the jet, as in the unlikely case of steady precession. Interpretation of the bends is complicated by the fact that they may be very less pronounced than they appear. If the jet is near the line of sight as suggested by the superluminal motions, even small bends can appear very large in projection.

VI. CONCLUSIONS

The major observational conclusions of this study are:

1. The radio emission from 3C 120 shows structure on all scales from less than a parsec to greater than 400 kpc.
2. There is a continuously connected jet visible from less than a parsec from the central engine to over 100 kpc, well outside the galaxy.
3. There is a lobe in the counterjet direction and diffuse emission in several directions. The lobe could be the outer portions of a counterjet seen along its axis, as suggested by its spectral index.
4. The three-dimensional morphology is not clear but might resemble some of the large double or wide-angle head-tail sources seen along the axis of the jet.
5. The polarization observations imply a longitudinal magnetic field throughout nearly all of the jet. Any Faraday rotation or depolarization is too small to be detected in these observations.
6. The brightness of the jet decreases following a simple power law with width. This implies that the physical parameters also follow simple power laws. It appears that the basic parameters of the jet are established near the core and are maintained throughout its length.

The observational conclusions, when interpreted in the context of the incoherent synchrotron model for the emission of the radio radiation, give the following results.

1. The minimum energy density drops at a rate close to proportional to the area of the jet. This implies that the minimum energy content per unit length of jet remains nearly constant throughout its length.
2. The magnetic field under the minimum energy assumption is proportional to the inverse of the jet width. This is the rate expected for flux-conserving expansion of a jet with a transverse magnetic field but is much slower than the rate expected for flux-conserving expansion of a jet with the longitudinal field implied by the polarization observations.
3. The velocity of the kiloparsec scale jet is still not clear. Energy balance arguments suggest that it is greater than $0.01c$. Relativistic velocities are required on parsec scales by the observation of superluminal motions and would naturally explain the one-sidedness of the kiloparsec scale structure. However, there is no firm evidence for or against relativistic velocities on the large scales.
4. The jet is likely to be light—it does not contain much thermal material. The density may be dominated by the relativistic electrons and associated protons.

So what is happening in 3C 120? Unfortunately the extensive data presented here do not suggest a definite model. Understanding even crude parameters such as density and velocity in extragalactic jets seems to be very difficult. Perhaps the simplest model consistent with the data is that a beam of relativistic gas, moving at relativistic speeds and containing no thermal gas, is generated on subparsec scales. It propagates at nearly constant velocity to a distance of about 100 kpc, expanding to maintain pressure balance with an external medium whose pressure decreases reasonably smoothly with distance from the center of the galaxy. The data, except for the measured polarization direction, are also consistent with an adiabatic jet that slows in the manner expected of a jet with a transverse magnetic field. As the jet approaches 100 kpc, it starts to break up and slow down. A counterjet with similar properties could exist and become visible as the southeast lobe when it slows. Knots appear at locations where the jet temporarily narrows, causing a rise in the energy density and, perhaps, shocks. The fact that the energy content per unit length is nearly constant suggests this simple scenario where both energy input and losses for the radiating gas are minor. Particle acceleration is not required in the outer regions of the jet, but the observed particles probably had to be reaccelerated after leaving the subparsec scales.

The fact that the jet maintains its character over so many orders of magnitude in size is one of the most important results of these observations. Most attempts to model astrophysical jets involve calculations of what happens over about an order of magnitude in scale size. Any such models that lead to a breakup of the jet in that range cannot apply to anything but the outer regions of real jets. The basic mechanisms that maintain the propagation and confinement of astrophysical jets must be capable of operating over many orders of magnitude. Also the properties of the external medium with which the jet interacts must scale relatively smoothly from parsec scales, deep in the nucleus of the galaxy, to well outside the galaxy.

It is tempting to treat the results presented in this paper on the connectedness of the jet and on the simple evolution of the physical parameters as evidence for what happens in other extragalactic sources. But is this extrapolation justified? A brightness decrease proportional to the square of the distance from the core is well matched to our observing equipment. If the decrease were faster, it is likely that the ratio of the extended emission to the emission of the compact core would be so low that the extended emission would not be seen. Compact sources with little or no extended emission are seen. BL Lac and DA 193 appear to be examples (our calibration data; Perley 1982). On the other hand, if the decrease were slower, the outer structure would dominate and studies of the inner jet would be difficult. The large radio galaxies such as Cygnus A (see Perley, Dreher, and Cowan 1984) are in this category. Certainly, there are many sources that do not evolve in the same way with distance as 3C 120. More sources will have to be studied in equivalent detail before we know how general the phenomena seen in 3C 120 are. However, despite the possible variety of structures, the basic lesson that the properties of jets must be considered over a very wide range of scales clearly applies to most sources. Any complete description of jet physics must cover the full range of scales.

A final, visual summary of the mapping effect is given in Figure 21 which is a montage of some of the maps in this paper, all shown on one sheet with the relationship between the various maps clearly indicated.

The authors would like to thank Alan Bridle, Jean Eilek, Phil Hardee, Chris O'Dea, Frazer Owen, Rick Perley, and Joan Wrobel for useful information and stimulating discussions. We would also like to thank Tim Cornwell for ideas and advice that led to the first successful (i.e., leading to improvements in a map) application of closure corrections to VLA data. We thank Joan Wrobel and Rick Perley for critical readings of the manuscript. The VLBI program at Owens Valley Radio Observatory is supported by the National Science Foundation.

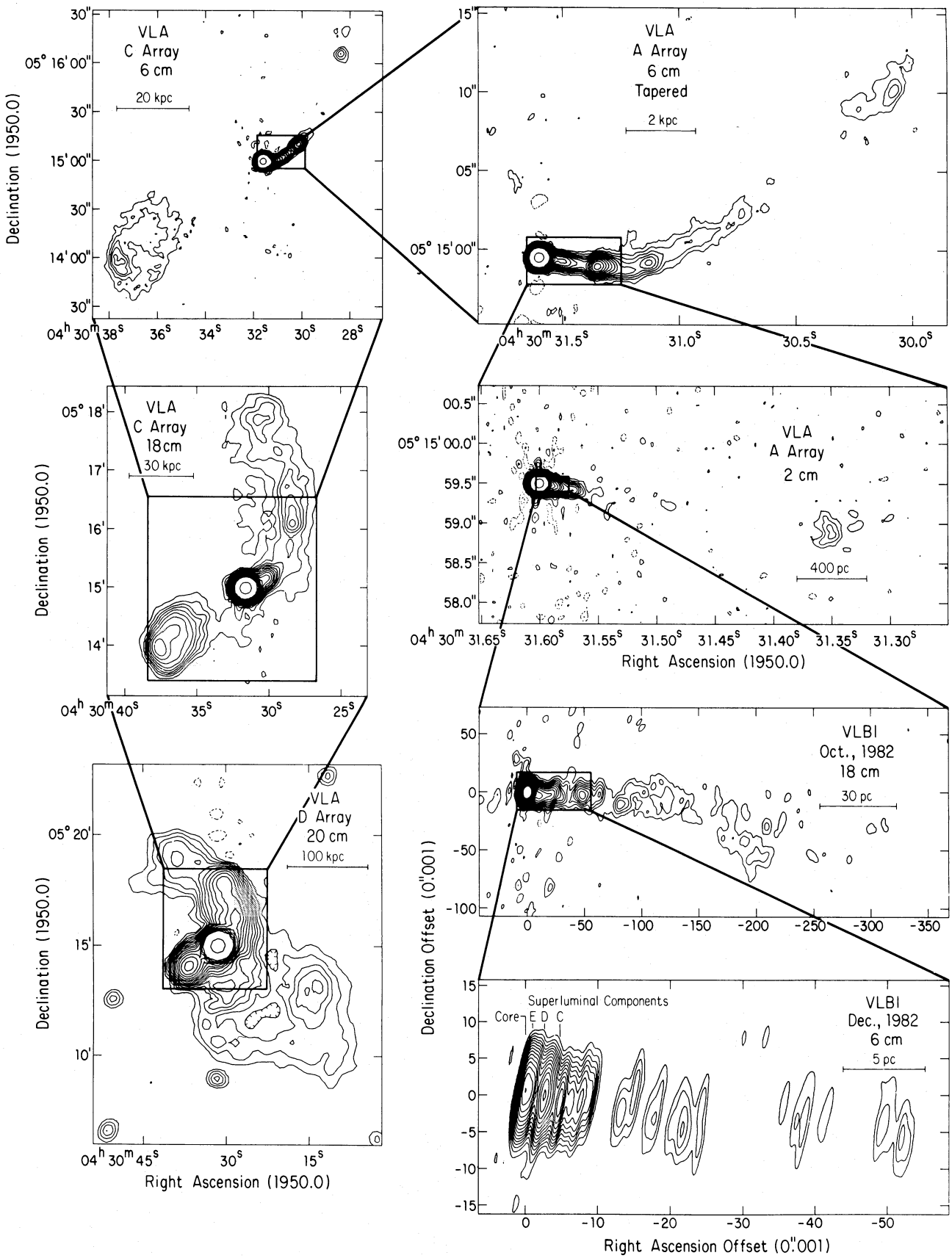

FIG. 21.—A montage of some of the maps of 3C 120 presented elsewhere in this paper. The relationship between maps at successive resolutions is indicated by a box on each map showing the field-of-view of the next higher resolution map and lines from that box to the corresponding map.

APPENDIX

The key to the very high dynamic ranges obtained for many of the maps presented in this paper is the corrections that were made for closure errors. The usual VLA and VLBI calibration methods assume that the amplitudes and phases of all baselines can be calibrated by finding one set of gains for each antenna. It is assumed that there are no baseline-dependent effects. Closure errors are the result when this assumption breaks down, as it does at some level for any real instrument. Some possible sources of closure errors are mismatched bandpasses, pointing errors on a large source, delay errors, and correlator errors. On the VLA, there appear to be closure errors at the level of a fraction of a percent that are sufficiently constant over periods of several hours that efforts to correct them give significant improvements to maps whose dynamic range is limited by them. As a rule of thumb, if the ratio of the peak to the off-source rms in a VLA map based on long tracks is 10,000, the dynamic range cannot be improved without closure corrections. If the dynamic range is not that high, closure corrections will not help. Closure errors can give a very distinctive signature on maps of a low declination, point-dominated source such as 3C 120—the noise to the north and south of the bright point is much higher than in other directions. It was the effort to get rid of this rather displeasing effect that led to attempts to correct for the closure errors.

The closure errors were corrected with the help of strong, very compact calibrators. Either 3C 84 or DA 193 (0552 + 398) was used for the maps presented here. The calibrator was observed for a total of 0.5 to 1 hr in order to obtain high signal-to-noise ratio data. The calibrator data were self-calibrated either assuming the source to be a point, or using CLEAN components of the best map that could be made from the data without closure corrections. The self-calibrated data were then divided by the predicted data based on the model (point source or CLEAN components) and averaged to give one point per IF per baseline. The numbers in the data set at this stage were amplitudes near 1.0 and phases near zero. The offsets from these values were the closure errors. The 3C 120 data were then divided by the closure errors. After this calibration, the high north-south noise was dramatically reduced and dynamic ranges (peak to off source rms) up to 30,000 were achieved (50,000 if the rms measurement region did not include any of the region affected by the north-south problems). The procedure described here is not capable of correcting closure errors in the polarization data, so the dynamic range of the polarization maps is lower than that of the total intensity maps. This is offset somewhat by the fact that the peak flux density in the polarization maps is well below that in the total intensity maps. However, in practice, the noise level in the polarization maps was above that in the total intensity maps.

As a test, the closure corrections that had been used to improve maps based on real data were applied to artificial data. The artificial data were very similar to the real data except they were not subject to closure errors and did not contain noise. The same *u-v* coverage was used as for the real data and the model source used to generate the artificial data consisted of clean components from the map based on the real data. The unaltered artificial data produced a map with a peak to rms ratio of 100,000 (limited by use of two byte integers). When the artificial data were corrupted by application of the closure corrections, the peak to rms ratio dropped to 10,000. This should represent an upper limit to the dynamic range of a map based on corrected data unless the corrections are actually removing problems in the data. Since the real data produced significantly higher dynamic ranges after the corrections were applied (but not before), it is clear that the corrections were useful. A more complete description of what was done and some before and after displays can be found in a VLA Scientific Memorandum (Walker 1984*b*).

The above calibration was accomplished within the AIPS data reduction package at the NRAO. For a point source model, the self-calibration and division steps can be combined by giving ASCAL (the self-calibration program) a 1.0 Jy point source as a model and allowing the gains to float.

It should be pointed out that the above procedure for correcting closure errors can be misused. The extreme example would be to use a source as its own closure calibrator for short-duration observations. The procedure will produce an extremely high "dynamic range" map, but it will be an exact reproduction of the assumed source model and will contain no new information. More subtly, the procedure can attempt to transfer any unmodeled structure from the calibrator source to the program source, especially if the *u-v* coverage is similar. With very dissimilar coverage, the effects are less obvious and are most likely just to degrade the effectiveness of the attempted calibration. In fact, for the 1.4 GHz, A-configuration observation presented in this paper, the initial closure calibration was made using a point source model for 3C 84. The calibration did not help the 3C 120 map. However, when a map was made of 3C 84, it became obvious that the point source was a poor model. When a better 3C 84 model was used, the 3C 120 map improved considerably.

REFERENCES

Aller, H. D., Olsen, E. T., and Aller, M. F. 1976, *A.J.*, **81**, 738.
Arp, H. 1981, in *Proc. 2nd ESO/ESA Workshop, Optical Jets in Galaxies*, ed. B. Battrick and J. Mort (Paris: European Space Agency), p. 53.
———. 1986, preprint.
Baars, J. W. M., Genzel, R., Pauliny-Toth, I. I. K., and Witzel, A. 1977, *Astr. Ap. Suppl.*, **61**, 99.
Baldwin, J. A., Carswell, R. F., Wampler, E. J., Smith, H. E., Burbidge, E. M., and Boksenburg, A. 1980, *Ap. J.*, **236**, 388.
Balick, B., Heckman, T. M., and Crane, P. C. 1982, *Ap. J.*, **254**, 483.
Begelman, M. C., Blandford, R. D., and Rees, M. J. 1984, *Rev. Mod. Phys.*, **56**, 255.
Benford, G. 1984, in *Physics of Energy Transport in Extragalactic Radio Sources* (N.R.A.O. Workshop No. 9), ed. A. H. Bridle and J. A. Eilek (Green Bank: N.R.A.O.), p. 185.
Benson, J. M., Walker, R. C., Seielstad, G. A., and Unwin, S. C. 1984, in *IAU Symposium 110, VLBI and Compact Radio Sources*, ed. R. Fanti, K. Kellermann, and G. Setti (Dordrecht: Reidel), p. 125.
Benson, J. M., Walker, R. C., Unwin, S. C., Booth, R., and Pilbratt, G. 1986, in preparation (Paper II).
Blandford, R. D., and Königl, A. 1979, *Ap. J.*, **232**, 34.
Bridle, A. H., and Perley, R. A. 1984, *Ann. Rev. Astr. Ap.*, **22**, 319.
de Bruyn, A. G., and Schilizzi, R. T. 1984, in *VLBI and Compact Radio Sources*, ed. R. Fanti, K. Kellermann, and G. Setti (Dordrecht: Reidel). p. 165.
Eilek, J. A., Burns, J. O., O'Dea, C. P., and Owen, F. N. 1984, *Ap. J.*, **278**, 37.
Ekers, R. D., Fanti, R., Lari, C., and Parma, P. 1981, *Astr. Ap.*, **101**, 194.
Epstein, E. E., Fogarty, W. G., Mottmann, J., and Schneider, E. 1982, *A.J.*, **87**, 449.
Fabian, A., and Kembhavi, A. 1982, in *IAU Symposium 97, Extragalactic Radio Sources*, ed. D. S. Heeschen and C. M. Wade (Dordrecht: Reidel), p. 453.
Ferland, G. J., and Shields, G. A. 1985, in *Astrophysics of Active Galaxies and Quasistellar Objects*, ed. J. S. Miller (Mill Valley, CA: University Science Books). p. 157.
Forman, W., Jones, C., and Tucker, W. 1985, *Ap. J.*, **293**, 102.
Gower, A. C., Gregory, P. C., Hutching, J. B., and Unruh, W. C. 1982, *Ap. J.*, **262**, 478.
Halpern, J. P. 1984, *Ap. J.*, **290**, 130.
Hardee, P. E. 1984, *Ap. J.*, **287**, 523.

Högbom, J. A. 1974, *Astr. Ap. Suppl.*, **15**, 417.
Kraus, J. D. 1966, *Radio Astronomy* (New York: McGraw-Hill).
Linfield, R., and Perley, R. 1984, *Ap. J.*, **279**, 60.
Lyutyi, V. M. 1979, *Soviet Astr.*, **23**, 518.
Margon, B. 1984, *Ann. Rev. Astr. Ap.*, **22**, 507.
Miley, G. 1980, *Ann. Rev. Astr. Ap.*, **18**, 165.
Myers, P. C. 1978, *Ap. J.*, **225**, 380.
O'Dea, C. P. 1984, Ph. D. thesis, University of Massachusetts, Amherst.
O'Dea, C. P., and Owen, F. N. 1985, *A.J.*, **90**, 927.
Oke, J. B., Readhead, A. C. S., and Sargent, W. L. W. 1980, *Pub. A.S.P.*, **92**, 758.
Osterbrock, D. E. 1979, in *Active Galactic Nuclei*, ed. C. Hazard and S. Mitton (Cambridge: Cambridge University Press), p. 25.
Owen, F. N., Hardee, P. E., and Bignell, R. C. 1980, *Ap. J. (Letters)*, **239**, L11.
Pacholczyk, A. G. 1970, *Radio Astrophysics* (San Francisco: Freeman).
Perley, R. A. 1982, *A.J.*, **87**, 859.
Perley, R. A., Dreher, J. W., and Cowan, J. J. 1984, *Ap. J. (Letters)*, **285**, L35.
Pollock, J. T., Pica, A. J., Smith, A. G., Leacock, R. J., Edwards, P. L., and Scott, R. L. 1979, *Ap. J.*, **290**, 130.
Readhead, A. C. S., and Wilkinson, P. N. 1978, *Ap. J.*, **223**, 25.
Rieke, G. G., and Lebofsky, M. J. 1979, *Ap. J.*, **227**, 710.
Rudnick, L., and Edgar, B. K. E. 1984, *Ap. J.*, **257**, 63.
Schilizzi, R. T., and de Bruyn, A. G. 1983, *Nature*, **303**, 26.
Schwab, F. R. 1980, *SPIE Proc.*, **231**, 18.
Seielstad, G. A., Cohen, M. H., Linfield, R. P., Moffet, A. T., Romney, J. D., Schilizzi, R. T., and Shaffer, D. B. 1979, *Ap. J.*, **229**, 53.
Soboleva, N. S., Berlin, A. A., Nizhel'skii, N. A., and Spangenberg, E. E. 1982, *Soviet Astr. Letters*, **8**, 108.
Spitzer, L. 1978, *Physical Processes in the Interstellar Medium* (New York: Wiley).
Thompson, A. R., Clark, B. G., Wade, C. M., and Napier, P. J. 1980, *Ap. J. Suppl.*, **44**, 151.
Unwin, S. C., Cohen, M. H., Biretta, J. A., Pearson, T. J., Seielstad, G. A., Walker, R. C., Simon, R. S., and Linfield, R. P. 1985, *Ap. J.*, **289**, 109.
Unwin, S. C., Cohen, M. H., Pearson, T. J., Seielstad, G. A., Simon, R. S., Linfield, R. P., and Walker, R. C. 1983, *Ap. J.*, **271**, 536.
van Breugel, W., Filippenko, A. V., Heckman, T., and Miley, G. 1985, *Ap. J.*, **293**, 83.
Walker, R. C. 1984*a*, in *Physics of Energy Transport in Extragalactic Radio Sources* (N.R.A.O. Workshop No. 9), ed. A. H. Bridle and J. A. Eilek (Green Bank: N.R.A.O.), p. 20.
Walker, R. C. 1984*b*, *VLA Scientific Memorandum No. 152* (Socorro: National Radio Astronomy Observatory).
Walker, R. C., Benson, J. M., Seielstad, G. A., and Unwin, S. C. 1984, in *IAU Symposium 110, VLBI and Compact Radio Sources*, ed. R. Fanti, K. Kellermann, and G. Setti (Dordrecht: Reidel), p. 121.
Walker, R. C., Benson, J. M., Unwin, S. C., and Seielstad, G. A. 1986, in preparation (Paper 1).
Walker, R. C., Seielstad, G. A., Simon, R. S., Unwin, S. C., Pearson, T. J., and Linfield, R. P. 1982, *Ap. J.*, **257**, 56.
Wardle, J. F. C. 1977, *Nature*, **269**, 563.
Wardle, J. F. C., and Potash, R. I. 1984, in *Physics of Energy Transport in Extragalactic Radio Sources* (N.R.A.O. Workshop No. 9), ed. A. H. Bridle and J. A. Eilek (Green Bank: N.R.A.O.), p. 30.
Willis, A. G., Strom, R. G., and Wilson, A. S. 1974, *Nature*, **250**, 624.
Wlerick, G., Bouchet, P., Cayatte, V., and Michet, D. 1981, *Astr. Ap.*, **102**, L17.
Wlerick, G., Westerlund, B., and Garnier, R. 1979, *Astr. Ap.*, **72**, 277.

J. M. BENSON: National Radio Astronomy Observatory, Edgemont Rd., Charlottesville, VA 22901

S. C. UNWIN: Owens Valley Radio Observatory, California Institute of Technology, Mail Code 105-24, Pasadena, CA 91125

R. C. WALKER: National Radio Astronomy Observatory, P.O. Box O, Socorro, New Mexico 87801